# Application of a combination of dating techniques to reconstruct the Lateglacial and early Holocene landscape history of the Albula region (eastern Switzerland)

Böhlert, R ; Egli, M ; Maisch, M ; Brandova, D ; Ivy-Ochs, S ; Kubik, P W ; Haeberli, W

Abstract: Landforms in Val Mulix and the Albula region in eastern Switzerland offer a detailed insight into the period between the Oldest Dryas until the early Holocene. To better understand Lateglacial and Holocene climate change in the central Alps, glacial (moraines, polished bedrock) and periglacial (rock glacier) landforms were dated using a combined approach of numerical (cosmogenic 10Be) and relative (Schmidt-hammer, weathering rind thickness) dating techniques. At high-elevation sites near the Last Glacial Maximum (LGM) trimline, 10Be exposure ages of glacially modified bedrock are between 11.2 ka and 13.5 ka. This suggests the persistence of long-lasting small local ice caps after the breakdown of the LGM ice domes or, alternatively, a reformation of ice perhaps during the Younger Dryas. In Val Mulix we obtained one of the first ages for the Daun-stadial (> 14.7 ka) moraines (14.9 ± 1.8 ka), supporting a pre-Bølling chronological position. The age is in excellent agreement with the age of a boulder from an Egesen I moraine located up-valley which we postulate may be a Daun moraine that was re-occupied during the Egesen stadial. A boulder from an Egesen II moraine gave an age of 10.7 ka, which is similar to ages of Egesen II moraines at other sites in the Alps. 10Be ages from boulders found on a relict rock glacier in Val Mulix indicate that the main active phase lasted from the Lateglacial until the early Holocene. The derived mean annual flow rate is of the order of decimetres, which is in accordance with values stated in the literature based on measuring active rock glaciers in the Alps. Exposure ages from a glacially polished rock barrier showed that this area was ice-free at the end of the Younger Dryas (9.0 ± 0.7 ka and 11.9 ± 0.9 ka). The polished bedrocks are located a few hundred meters down-valley from the Little Ice Age (LIA) moraines. This gives direct evidence of a fast ice retreat towards the end of the Younger Dryas, with glacier length variations that did not exceed the 1850 AD extension (Little Ice Age maximum). Surface exposure dating is, however, limited by several methodological constraints. The choice of suitable snow depths plays a crucial role in the calculation of the 10Be ages. Shielding of surfaces from cosmic rays by snow can significantly influence the exposure age, and variations in the estimated annual snowfall in the Albula region since the LGM is therefore a potential source of considerable uncertainty in our measurements. While the measurement of weathering rind thicknesses turned out to be an appropriate tool to support the reconstruction of Lateglacial landscape evolution, Schmidt-hammer R-values were less helpful. The R-values enabled a temporal distinction of landforms within the Holocene (LIA moraine, active rock glaciers) but not within the Lateglacial. From a methodological point of view, the different dating methods enabled a cross-checking, an extended interpretation of the data and a more accurate estimate of the possible sources of error.

DOI: https://doi.org/10.1016/j.geomorph.2010.10.034

Journal Article
Accepted Version

Originally published at:
Böhlert, R; Egli, M; Maisch, M; Brandova, D; Ivy-Ochs, S; Kubik, P W; Haeberli, W (2011). Application of a combination of dating techniques to reconstruct the Lateglacial and early Holocene landscape history of the Albula region (eastern Switzerland). Geomorphology, 127(1-2):1-13.
DOI: https://doi.org/10.1016/j.geomorph.2010.10.034

# Application of a combination of dating techniques to reconstruct the Lateglacial and early Holocene landscape history of the Albula region (eastern Switzerland)

Ralph Böhlert[1], Markus Egli[1], Max Maisch[1], Dagmar Brandová[1], Susan Ivy-Ochs[1,2], Peter W. Kubik[2], Wilfried Haeberli[1]

[1]Department of Geography, University of Zurich, CH-8057 Zurich, Switzerland

[2]Laboratory of Ion Beam Physics, ETH Zurich, CH-8093 Zurich, Switzerland

*E-mail to the corresponding author: ralph.boehlert@geo.uzh.ch

## Abstract

Landforms in Val Mulix and the Albula region in eastern Switzerland offer a detailed insight into the period between the Oldest Dryas until the early Holocene. To better understand Lateglacial and Holocene climate change in the central Alps, glacial (moraines, polished bedrock) and periglacial (rock glacier) landforms were dated using a combined approach of numerical (cosmogenic $^{10}$Be) and relative (Schmidt-hammer, weathering rind thickness) dating techniques.

At high-elevation sites near the Last Glacial Maximum (LGM) trimline, $^{10}$Be exposure ages of glacially modified bedrock are between 11.2 ka and 13.5 ka. This suggests the persistence of long-lasting small local ice caps after the breakdown of the LGM ice domes or, alternatively, a reformation of ice perhaps during the Younger Dryas.

In Val Mulix we obtained one of the first ages for the Daun-stadial (> 14.7 ka) moraines (14.9 ± 1.8 ka), supporting a pre-Bølling chronological position. The age is in excellent agreement with the age of a boulder from an Egesen I moraine located up-valley which we postulate may be a Daun

moraine that was re-occupied during the Egesen stadial. A boulder from an Egesen II moraine gave an age of 10.7 ka, which is similar to ages of Egesen II moraines at other sites in the Alps. $^{10}$Be ages from boulders found on a relict rock glacier in Val Mulix indicate that the main active phase lasted from the Lateglacial until the early Holocene. The derived mean annual flow rate is of the order of decimetres, which is in accordance with values stated in the literature based on measuring active rock glaciers in the Alps. Exposure ages from a glacially polished rock barrier showed that this area was ice-free at the end of the Younger Dryas (9.0 ± 0.7 ka and 11.9 ± 0.9 ka). The polished bedrocks are located a few hundred meters down-valley from the Little Ice Age (LIA) moraines. This gives direct evidence of a fast ice retreat towards the end of the Younger Dryas, with glacier length variations that did not exceed the 1850 AD extension (Little Ice Age maximum). Surface exposure dating is, however, limited by several methodological constraints. The choice of suitable snow depths plays a crucial role in the calculation of the $^{10}$Be ages. Shielding of surfaces from cosmic rays by snow can significantly influence the exposure age, and variations in the estimated annual snowfall in the Albula region since the LGM is therefore a potential source of considerable uncertainty in our measurements. While the measurement of weathering rind thicknesses turned out to be an appropriate tool to support the reconstruction of Lateglacial landscape evolution, Schmidt-hammer R-values were less helpful. The R-values enabled a temporal distinction of landforms within the Holocene (LIA moraine, active rock glaciers) but not within the Lateglacial. From a methodological point of view, the different dating methods enabled a cross-checking, an extended interpretation of the data and a more accurate estimate of the possible sources of error.

**Keywords:** Lateglacial landscape evolution, dating methods, cosmogenic $^{10}$Be, Schmidt-hammer, weathering rinds

## 1. Introduction

The analysis and dating of natural climate archives allows for the determination of past climatic conditions and rates of geomorphologic processes. This can serve as a basis for modelling and predictions of future landscape states. Moraines contain the only direct evidence of past glacier fluctuations, that are highly sensitive to climate changes (e.g. Oerlemans et al., 1998; Haeberli, 2004). In order to address the question of global synchrony of cold/warm cycles, the correlation of the terrestrial record with deep-sea sediment and ice core records is of central importance. This requires reliable, accurate dating.

The 'Alpine Lateglacial' is defined after Penck and Brückner (1901/1909) as the time period between the final disintegration of the foreland piedmont glaciers (Schlüchter, 2004) formed during the Last Glacial Maximum (LGM, around 21 ka: Ivy-Ochs et al., 2004) and the beginning of the Holocene (around 11.6 ka). Several distinct moraine complexes along mountain valleys and in cirques characterise this time span. These glacial remnants resulted from repeated glacier re-advances ('stadials') interrupting the ice retreat. They record the unstable behaviour of climate during this time of general ice recession. Geomorphological mapping based on relative moraine positions, moraine morphology and the calculation of equilibrium line altitude depression (ΔELA, based on a Accumulation Area Ratio AAR = 0.67, all ΔELA values given refer to the Little Ice Age (LIA) extension) supported by $^{14}$C-dating of related peat bogs gave rise to the possibility of assigning moraines to different stadials (Gross et al., 1977; Kerschner, 1978; Maisch, 1981; Suter, 1981; Keller and Krayss, 1993, 2005; Kerschner et al., 1999). With improvements in the dating technique using *in situ* produced cosmogenic isotopes in rock surfaces (Lal, 1988), the direct determination of moraine ages (Gosse and Phillips, 2001) became possible at sites where there is no available organic material for $^{14}$C determinations. Since then, a great number of studies have been performed with the aim of dating moraines and associated glacier fluctuations using cosmogenic

nuclides, especially $^{10}$Be (see compilation in Reuther et al., 2006). Ivy-Ochs et al. (2006) provide a summary of cosmogenic nuclide exposure ages for the Lateglacial focusing on the European Alps. The time span considered here includes the Oldest Dryas (c. 19 – 14.7 ka) and the Bølling-Allerød interstadial (c. 14.7 – 12.9 ka), followed by the Younger Dryas (12.9 – 11.6 ka) and the subsequent transition to the Holocene (approximate ages are based on Ivy-Ochs et al., 2008). Based on an increasing number of exposure dates (Ivy-Ochs et al., 2009a) it is generally accepted that the Egesen stadial complex (Heuberger, 1966) can be correlated to the Younger Dryas cold phase. For older glacier stages and particularly for the Daun (Heuberger, 1966) and the Clavadel/Senders stadial moraines (Maisch, 1981; Kerschner and Berktold, 1982) – morphostratigraphically preceding the Younger Dryas moraines – age constraints are rare (Ivy-Ochs et al., 2008). In addition, although initial results have been presented (e.g. Ivy-Ochs et al., 2006, 2007; Kelly et al., 2006, Cossart et al., 2010), the absolute chronology for glacial erosional features at higher altitudes near the trimline that potentially includes information about the early breakdown of the LGM ice domes is poorly established.

The aim of this study is to improve the understanding of the Lateglacial and early Holocene chronology by dating both glacial (moraines, glacially polished bedrock) and periglacial (rock glacier) landforms with surface exposure dating using $^{10}$Be. In this study we compare numerical and relative dating methods, such as Schmidt-hammer rebound values and weathering rind thicknesses, applying both to the same landforms where possible. Schmidt-hammer and weathering rind measurements have, in particular, proven their usefulness in geomorphology, especially on landforms that developed during the Holocene and partially also for landforms attributed to the Lateglacial period (e.g. Oguchi, 2001; Shakesby et al., 2006; Engel, 2007). The combined application of both relative and absolute (numerical) dating methods opens the possibility of calibrating the relative methods and enables the estimation of possible error sources (Haeberli et al., 2003).

## 2. Study area and sampling sites

### 2.1. Study area characteristics

The investigated area, which includes Val Mulix and the region to the west of Albulapass, is located in the eastern part of the Swiss Alps, c. 30 km south of the city of Chur (Fig. 1). Hypothetical assignments of moraines in our study area to a given stadial (such as Egesen and Daun), as shown in Fig. 1, are based on the work of Maisch (1981). Sample sites and corresponding analyses are listed in Table 1.

Tectonically the region is situated within the Err-Bernina nappe that belongs to the lower Austroalpine (Pfiffner, 2009). The greenish 'Albula Granite' comprised of quartz, plagioclase (in places altered to epidote), k-feldspar, biotite and rarely hornblende is the dominant rock type (Cornelius, 1929, 1935; Bearth et al., 1987). The adjacent area to the north of Albulapass belongs to the Ela nappe, composed mainly of sedimentary rock types. Mean annual precipitation varies between c. 1200 mm in the lower parts near Preda (Fig. 1) and up to 1800 mm towards the mountain ridges (EDI, 1992; Schwarb et al., 2000). The reconstructed LGM ice surface geometry that is based on glaciomorphic mapping shows that the area was situated near the 'Engadine ice dome' that was centred in the Upper Engadine. Trimline and other erosional features indicate that during the LGM the Albulapass formed a northward transfluence with ice flowing from Engadine into the Rhine river system (Florineth, 1998; Florineth and Schlüchter, 2000; Bini et al., 2009).

### 2.2. Description of the sampled sites

125 The area near Albulapass is characterised by three distinct elevation levels of polished bedrock,
126 namely at Bottas Glischas, Crap Alv Laiets and Crap Alv at c. 2600, 2300 and 2000 m asl,
127 respectively (Fig. 1, 2D). Bottas Glischas is a well-pronounced transfluence saddle near the trimline
128 (Fig. 2C). Traces of glacial erosion and plucking processes show that LGM ice flowed northwards
129 from Val Bever into the Albula catchment. This site is particularly suitable to highlight the timing
130 of the breakdown of the LGM Engadine ice dome as the sampled bedrock surfaces lie outside of
131 possible influence of local cirque glaciers. Following collapse of the LGM ice domes, ice masses
132 separated into a topography-dominated ice-flow system of interconnected valley glaciers.
133 According to palynological analyses of a nearby peat bog ('Peat bog' in Fig. 1) (Burga in Maisch,
134 1981), the roche moutonnée at Crap Alv (Fig. 1, 2D) became ice free at the latest towards the end of
135 the Allerød interstadial. Accordingly, the roche moutonnée can be positioned within the former
136 tongue area of the Daun glaciation. Moraine fragments (highlighted as 'Daun' in Fig. 1) allow for
137 the reconstruction of a Daun-equivalent glacier position with an ELA depression value of 260 m
138 (Maisch, 1981). This value is slightly higher than those usually measured for the Younger Dryas
139 and lower than those usually measured for the Daun stadial (part of the Oldest Dryas). In order to
140 clarify this situation, the roche moutonnée (Alb 7 and 8; Fig. 1) at this site was dated and a boulder
141 was sampled for surface exposure dating (Cra1) on a moraine located 500 m up-valley from the
142 roche moutonnée at Crap Alv. The Cra1 moraine was most probably deposited during the Egesen
143 stadial (Younger Dryas; Maisch, 1981). Both Schmidt-hammer measurements and exposure dating
144 using $^{10}$Be were applied on all three bedrock elevation levels (sample code Alb, see Fig. 1 and
145 Table 1). Considering the potential influence of aspect on the early Lateglacial ice melt, sample
146 Alb10 was taken on the south slope of Bottas Glischas 95 m below the highest transfluence point.
147 An additional sample (Alb6) for surface exposure dating was taken at the nearby Fuorcla Melnetta
148 (Fig. 1).

149 In Val Mulix, numerous landforms from the Lateglacial and the early Holocene time period can be
150 found (Fig. 1), suggesting several readvances of glaciers. The hamlet of Naz is situated between
151 several moraine fragments that together clearly represent a terminal glacier position. Based on the
152 classification of Maisch (1981) they are attributable to the Daun stadial, with an ELA depression of
153 345 m. Other Daun moraines are located on the south slope of Val Tschitta and at the former
154 confluence point of Val Tschitta and the Val Mulix glacier. A boulder having a height of c. 1.5 m
155 on the latter moraine was sampled for exposure dating (VM7). This moraine is strongly vegetated
156 (dwarf-shrubs and pines) and shows well-developed soil formation. Boulders are almost completely
157 absent here.
158 The well-preserved moraines in the Val Tschitta and the Val Mulix, believed to be Egesen
159 equivalents, show ELA depression values of ~220 and ~230 m (Maisch, 1981), respectively.
160 Generally, the moraines in this area are mostly well preserved. The Egesen I terminal moraine is
161 sharp crested but block sizes are small (diameters of ≤ 80 cm) and no boulder acceptable for
162 exposure dating could be found. The lateral moraines (upper and lower Egesen I) are less blocky
163 and soil development is more advanced. Boulders on top of the moraine crests are rather sparse.
164 The upper Egesen I moraine slopes down several hundred metres (from 2300 m to 2100 m asl) to
165 the valley bottom of Val Mulix. The lower Egesen I moraine is less pronounced but still clearly
166 identifiable as a distinct moraine. On its lower part, this moraine is strongly subjected to slope creep
167 processes. This is not the case for the part where it was sampled for exposure dating. Samples for
168 exposure dating were taken on the upper (VM1) and the lower Egesen I moraine (VM4) (Fig. 2B).
169 A very blocky moraine about 1 km further up-valley in Val Mulix (Fig. 1), having a ELA
170 depression of 125 m, can be classified as Egesen II or as Bocktentälli substadial, according to the
171 local nomenclature in this area (Maisch, 1981). The moraine is sharp-crested and consists of coarse
172 blocks. As this moraine was deposited in a flat area, post depositional processes leading to moraine
173 degradation can be ruled out. On the Egesen II moraine, two suitable boulders were found (VM6,

VM11). Weathering rinds were measured on the upper Egesen I and on the Egesen II moraines. Schmidt-hammer rebound values were also recorded on the Egesen I terminal moraine and on the 1850 AD moraine. Remarkable from a morphostratigraphic point of view is the situation on the orographically right-hand side (see Fig. 1, 2A) of the Mulix valley and consequently on the right border of the former Egesen I glacier. Here a mass of glacial sediments, perhaps ice-cored that was previously dammed behind the lateral Egesen I moraine, began to move downhill – most probably under permafrost conditions – and created a breach in this moraine. This must have occurred after the retreat of the main ice body of Egesen I. The rock glacier is therefore younger than the Egesen I stage. Maisch (1981) suggests that the main active phase occurred simultaneously to the Egesen II advance. At least at an initial stage, the source material could mainly have been provided by a higher altitude and deformed Daun moraine and the Egesen I moraine itself. Later on, an additional debris supply from the headwall must be assumed; otherwise the formation of an almost 700 m-long rock glacier is unlikely. According to the terminology of Frauenfelder (2005), this rock glacier can be characterised as a mixed 'moraine-derived' and 'talus-derived' form. Schmidt-hammer and weathering rind measurements were carried out in the uppermost, the middle and the lowermost part near the front of the rock glacier.

In the basin of Val Mulix, a glacially polished bedrock step (Sur la Crappa) divides the valley into two distinct elevation levels: one at 2400 m asl and one at 2200 m asl. The bedrock step is about 500 m down-valley from the LIA moraine of the Laviner glacier and 1 km up-valley from the Egesen II moraine. At this bedrock step we collected Schmidt-hammer measurements and samples for exposure dating (VM8, VM10).

## 3. Methods

### 3.1. Schmidt-hammer rebound values

The Schmidt-hammer is a portable instrument originally developed to test concrete quality in a non-destructive way (Schmidt, 1951). A spring-loaded bolt impacting a surface yields a rebound- or R-value, which is proportional to the hardness (compressive strength) of a rock surface. Applied in geomorphology, more weathered surfaces provide low R-values and less weathered surfaces correspondingly high R-values. Comparing Schmidt-hammer rebound values requires an identical rock type having comparable initial surface hardness and weathering resistance within the test site (McCarroll, 1987). Since the 1980s the method has also been successfully used for relative dating of geomorphologic features such as moraines (e.g. Matthews and Shakesby, 1984; Winkler and Shakesby, 1995; Winkler, 2005), rock glaciers (e.g. Frauenfelder et al., 2005; Kellerer-Pirklbauer, 2008; Kellerer-Pirklbauer et al., 2008) or rockfall deposits (Nesje et al., 1994). Recent publications increasingly discuss the possibilities and limitations of calibrating R-values, for instance with results from $^{10}$Be and $^{14}$C dating (e.g. Shakesby et al., 2006; Engel, 2007) or from photogrammetrical measurements on rock glaciers and derived age estimations deduced from streamline interpolations (Haeberli et al., 2003; Frauenfelder et al., 2005).

In this study the N-type Schmidt-hammer (Proceq, Switzerland) was used. On each mappable unit (e.g. moraine, rock glacier lobe) 50 randomly selected boulders/sites were measured, avoiding edges of boulders (Day and Goudie, 1977), spots having lichen growth and also areas having visual fissures or cracks. Only flat parts under dry conditions were considered. Normally just one measurement is carried out per boulder; however, in some cases with just a low number of suitable boulders, the biggest ones were measured at most three times. Following the suggestions of Winkler (2000), we used a standard error based on the standard deviation in a 95% confidence interval to obtain statistically significant age differences:

$$x \pm 1.96 \times \sqrt{\left(\sigma/\sqrt{n}\right)} \qquad (1)$$

where $x$ is the arithmetic mean, $\sigma$ the standard deviation and $n$ corresponds to the number of measurements.

### 3.2. Weathering rind thicknesses

Rock surfaces exposed to the atmosphere are subject to (biogeo-)chemical weathering processes that result in a coloured outer crust around the rock. For commonly-used definitions and methodological procedures see Oguchi (2001) and references therein. The time-dependent rind growth towards the rock-centre is used as an indicator of the relative ages of glacial and periglacial deposits. A great number of investigations have been carried out mainly on Holocene moraines and fluvial terraces having different lithologies in Western USA, New Zealand and Japan (e.g. Chinn, 1981; Colman and Pierce, 1981; Whitehouse et al., 1986). An extensive overview of previous studies on weathering rinds since the 1960s is given in Oguchi (2001). Limitations and potential error sources such as erosion are discussed thoroughly in Gordon and Dorn (2005).

At each site (top of moraines and rock glacier lobes) 50 rind samples were chipped using a hammer from boulders with a minimum diameter of c. 30-40 cm. The weathering rind was measured perpendicular to the surface using a 0.1 mm-graduated magnifying glass. Edges and cracks leading to larger rind thicknesses and an overestimation of weathering stages were avoided. Also rock pieces that showed weathering signs resulting from structural irregularities such as micro-cracks were omitted.

### 3.3. Exposure dating

248 Surface exposure dating with cosmogenic nuclides is based on the assumption that boulders were
249 transported by glaciers and were, since the time of the glacier retreat, exposed to cosmic rays
250 without being moved from their present position. Gosse et al. (1995) demonstrated that on a single
251 moraine the cosmogenic nuclide ages reflect the timing of deposition (see also Schaefer et al.,
252 2009).
253
254 *3.3.1. Sampling method*
255 All samples were removed using hammer and chisel and partly a battery-operated drill. We used
256 only the uppermost ≤ 5 cm of the rock surfaces.
257 We followed strict sampling requirements and sampled only boulders having a height of ≥ 1.5 m on
258 the top of moraine crests in order to ensure the highest possible geomorphological stability (Gosse
259 and Phillips, 2001; Ivy-Ochs and Schaller, 2010). Boulders that had possibly been covered by till
260 and eroded out after moraine stabilisation and also boulders having evidence of spalling were
261 avoided because it would lead to an underestimation of the effective exposure time (Reuther et al.,
262 2006; Ivy-Ochs et al., 2007). Because of possible edge effects (Masarik and Wieler, 2003),
263 marginal positions on sharply-shaped boulders were not sampled. Roche moutonnées were sampled
264 on or near their tops. Here, lichen types and degree of lichen coverage were helpful indicators of
265 snow influence and were used to identify areas that recently spalled. Often, only one boulder per
266 moraine large enough for surface exposure dating was found. We are aware of the fact that ages
267 obtained from different boulders on one and the same moraine may vary and that there is the
268 tendency especially to underestimate the true age (Putkonen and Swanson, 2003). From our point of
269 view, however, in the case of there being insufficient suitable boulders it was better to rely on just
270 one boulder having a suitable size and position rather than sampling a greater number of small and
271 possibly unstable or exhumed boulders. Furthermore, dating of additional associated landforms
272 gives a morphostratigraphical framework and minimises potential errors.

### 3.3.2. Sample preparation and age calculation

The samples were crushed, sieved and leached in order to obtain pure quartz following Kohl and Nishiizumi (1992) and Ivy-Ochs (1996). $^{9}$Be solution was added to the dried quartz, which was then dissolved in 40% HF. Be was isolated using anion and cation exchange columns followed by selective pH precipitation techniques (Ivy-Ochs, 1996). The $^{10}$Be/$^{9}$Be ratios were measured at the ETH Zurich Tandem Accelerator Mass Spectrometry (AMS) facility (Kubik and Christl, 2010). The $^{10}$Be concentrations (Table 5) are corrected for $^{10}$Be in the $^{9}$Be carrier solution ($1.68\pm0.20 \times 10^{-14}$) and are normalised to the ICN 01-5-1 AMS standard with a nominal $^{10}$Be/$^{9}$Be ratio of $2.709 \times 10^{-12}$ (Nishiizumi et al., 2007). The $^{10}$Be half-life used is 1.387±0.012 Ma (Korschinek et al., 2010; Chmeleff et al. 2010).

The surface exposure ages were calculated using a sea level and high latitude production rate of 4.58±0.27 $^{10}$Be atoms/gram $SiO_2$/year which includes 2.2 % production due to muon capture (Stone and Ballantyne, 2006; Nishiizumi et al., 2007). This production rate was scaled for latitude and altitude based on Stone (2000) and corrected for sample thickness assuming an exponential depth profile (Brown et al., 1992) with an effective radiation attenuation length of 160 g cm$^{-2}$ (Gosse and Phillips, 2001), a rock density of 2.65 g cm$^{-3}$ and a snow density of 0.3 g cm$^{-3}$. Erosion was assumed to be 3 mm ka$^{-1}$, based on cosmogenic nuclide data from granitic boulders on an LGM moraine in the northern Swiss foreland (Ivy-Ochs et al., 2004). Topographical (skyline) shielding was calculated based on Dunne et al. (1999) with a 25 m-grid DEM (source: swisstopo) and a geographical information system (ArcGIS 9.2). Geomagnetic field correction was omitted (Masarik et al., 200, Pigati and Lifton, 2004) because the effect is small in the Alps (max. 1-2%).

The choice of reasonable snow depths plays a crucial role in the calculation of $^{10}$Be ages, especially in the Alps. As directly applicable snow depth values from the past do not exist, they must be estimated, usually on very tentative evidence. A wide range of snow layer thicknesses is possible,

especially in the case of bedrock sites where snow accumulation is less restricted than on boulders. This leads to even more uncertainty. Fig. 3 shows that a theoretical error of 0.6 m in the snow depth estimation, which is not unlikely, would cause an age-shift of c. 800 years in the age range of our landforms. Taking the relatively short duration of Lateglacial oscillations into account, such errors are striking. If available, the integration of long-term snow measurements (as done in this study) allows the derivation of more objectively explainable maximum values. However, age uncertainties resulting from the assumption of similar snow depths during the entire Holocene and local effects due to boulder shape will remain. The snow cover in this study was estimated according to the mean of the November - April snow heights measured between 1983 and 2002 at three nearby weather stations (data source: Swiss Federal Institute for Snow and Avalanche Research, MeteoSwiss). The values from these three stations, all roughly at the same altitude, are comparable. Thus, a mean snow depth of 1.5 m during six months could be derived and seems to give a realistic value for 2500 m asl in this region. The theoretical snow height for each sample site was estimated using a mean snow depth gradient of 0.08 m/100 m altitude difference (Auer, 2003). We also considered boulder shape, wind exposure and surrounding vegetation. These factors lead to a reduction of snow depth compared to a flat area. In addition, satellite images taken in June from three different years (Spot images, 1993 - 1995) were compared with regard to the snow cover in the study area. Results from Bottas Glischas showed that, at least for some years, a longer-lasting snow cover needs to be considered. The derived recent snow cover is assumed to be representative for the entire Holocene.

Estimated errors are given at the 1$\sigma$ level, including the measurement error and the effects of altitude/latitude scaling, topography and depth. Mean ages given are arithmetic means with errors calculated as described in Ivy-Ochs et al. (2009b).

### 3.4 Chemical and mineralogical analyses

323 Measurement of the total element content of rock fragments was done using X-ray fluorescence
324 (XRF) (see Jenkins, 1999). Around 10 g of soil material were milled to < 50 µm in a tungsten
325 carbide disc swing mill (Retsch® RS1, Germany). Some 4 g of soil powder was mixed with 0.9 g of
326 Licowax® C Micro-Powder PM (Clariant, Switzerland), pressed into a 32 mm-pellet and analysed
327 using an energy dispersive X-ray fluorescence spectrometer (SPECTRO X-LAB 2000, SPECTRO
328 Analytical Instruments, Germany).
329 The quantitative mineralogical composition of the inorganic part of the fine earth of the parent
330 material (fraction < 2 mm) was obtained using Rietveld analysis (program AutoQuan/BGMN, GE
331 SEIFERT; Götze et al., 2004; Plötze et al., 2003) of XRD patterns of randomly oriented specimens
332 (Bruker AXS D8 Advance, Cu-Kα, 4-70° 2θ, 40kV, 40mA, 0.02°-steps, 4s/step, automatic theta
333 compensating divergence and anti-scattering slits, graphite monochromator).
334
335 **4. Results and discussion**
336
337 **4.1. Schmidt-hammer rebound values**
338
339 Schmidt-hammer rebound values (the arithmetic mean of 50 R-value records on each individual
340 landform) from both the Val Mulix and the region near the Albulapass are summarised in Table 2.
341 Generally the mean values scatter in a very small range. The results of the vertical sequence near
342 the Albulapass are shown in the lower part of Table 2. The mean values vary in the same range as in
343 the Val Mulix (upper part of Table 2). The roche moutonée Crap Alv (39.5 ± 1.9) could be
344 separated from the two other elevation levels (Crap Alv Laiets: 34.3 ± 1.9, Bottas Glischas: 33.3 ±
345 1.8) based on the significantly higher rebound values. This would mean that Crap Alv became ice-
346 free later than the other two elevation levels, assuming identical weathering and lithological

conditions at all sites (see also the following section). Taking the comparatively low time-resolution of the method into account, this interpretation should be treated with caution.

Considering the standard error after Winkler (2000), the differences between the Val Mulix sites are in most cases not statistically significant. The value of the terminal Egesen I moraine (Fig. 1) is, however, an exception. The higher value (41.0 ± 2.1) indicates a younger age compared, for instance, to the polished bedrock site at Sur la Crappa. From a morphostratigraphic point of view, this makes no sense and has consequently to be attributed to the method's inherent uncertainty. The value of the 1850 AD moraine (58.0 ± 1.9) clearly contrasts with those obtained from landforms that are assumed to be of Lateglacial age, the latter yielding R-values between 35 and 40. Castelli (2000), Laustela (2003), Frauenfelder et al. (2005) and Compeer (2009) measured Schmidt-hammer rebound on a number of active rock glaciers with identical lithology in and around the same area and obtained values varying from c. 40 – 45 near the terminus to 50 – 55 in the inception zone. This fits nicely into the gap between the Lateglacial values and those attributed to the LIA, supporting the assumption that active rock glaciers can be attributed to the Holocene (Fig. 4).

Although obtained from different surfaces (moraines, polished bedrock and glaciofluvial deposits) and varied metamorphic lithologies, Shakesby et al. (2006) found age intervals statistically different (95% confidence intervals) for the Little Ice Age, the Pre-Boreal and the Younger Dryas using Schmidt-hammer R-values. In the same study, a number of non-age-related factors, including operator bias, were identified as being of minor importance. Although the ranges of R-values differed slightly between the operators, they did not lead to systematic errors in the readings.

### 4.2. Weathering rind thicknesses

The histograms of weathering rind thickness from the five measured sites in Val Mulix are given in Fig. 5. Besides the absolute values, also the shape of the corresponding data histogram gives

information about surface age distribution. Asymmetric histograms with more than one peak (bi- to trimodal) and a broader distribution (right skewed) are typical for old surfaces. To represent weathering rind thicknesses in this study, both the median and the mean values are given.

The observed sequence of weathering rind growth is in line with the geomorphological settings in the Val Mulix (see Fig. 1) and, therefore, seems to be an appropriate tool for reconstructing the landscape evolution. Histogram shape and statistical values identify the upper Egesen I moraine (mean/median: 4.6 mm/4.0 mm) as the oldest landform investigated. The values of the lower Egesen II moraine (mean/median: 3.1 mm/3.1 mm) and those from the terminal area of the relict rock glacier are similar, strengthening the thesis of a relatively parallel evolution of these landforms (Maisch, 1981). The middle and upper part of the relict rock glacier cannot be clearly distinguished (mean/median: 2.6 mm/2.2 mm and 2.2 mm/2.1 mm, respectively). However, a distinct age separation of the uppermost part from the terminal area (mean/median: 2.9 mm/2.9 mm) is evident. This general tendency does not change if the ten lowest or alternatively the five highest and the five lowest values are excluded, since young surfaces are often generated by rock fracturing and the chance exists that boulders having pre-existing weathering rinds are deposited. Whereas the first case generally leads to ‘too young’ ages, the second case suggests a ‘too old’ age.

Our data agree well with the findings of Castelli (2000), Laustela et al. (2003) and Compeer (2009). They found median values between 1.5 and 2 mm on lobes near the front of active rock glaciers in the same area. This shows the capability of the technique to distinguish between relict rock glaciers and active ones.

Regarding the comparability and transferability of Schmidt-hammer and weathering rind measurements, it is important to note some necessary ancillary conditions. The geology of all sites within the study area and also of the neighbouring study sites to which reference is made is similar. Although being part of two different geological nappes, the considered granite is virtually identical regarding texture. The main chemical and mineralogical composition of rock and sand material of

some sites in Val Mulix are given in Tables 3 and 4. The rock, typically for granite, is Si- and Al-rich and has only a low content of base cations such as Ca, Mg, K and Na. All sampling sites in Switzerland to which the results of this study are compared are distributed over a similar altitude range of c. 500 m. They are situated at the meteorological divide between the more humid northern Alps and the drier region of the Engadine, a region subject overall to the same large-scale precipitation pattern. Based on that, we assume that the conditions for weathering processes are comparable between the sites.

### 4.3. Surface exposure dating using $^{10}$Be

Surface exposure ages were calculated as described in section 3.3.2. For comparison, we also calculated the exposure ages using the Cronus on-line age calculator (input data Table 5) (Balco et al., 2008). The difference in our results to those calculated using the scaling scheme for spallation (Lal, 1991; Stone, 2000) is -5 to -85 years and about ± 40 years using the time-dependent scaling scheme (Lal, 1991; Stone, 2000). Our estimated error (1 σ; see Table 6) compares very favourably with Cronus' internal uncertainty.

#### *4.3.1. Albula region*

The clearly pronounced trimline around 2800 m asl, especially the Crasta Mora to the east of Piz da las Blais (Fig. 1), indicates that the transfluence pass Bottas Glischas (~ 2600 m asl) must have been covered by at least 200 m of ice during the LGM. The overall morphology and the spatially homogeneous and freshly striated landforms imply a basal sliding of (at least at times) a warm-based glacier. The ages of 11.2 ± 0.9 (Alb9), 11.7 ± 1.3 (Alb10) and 13.5 ± 1.4 ka (Alb2) (Table 6, Fig. 6) at Bottas Glischas and 13.5 ± 1.4 ka (Alb6) at Fuorcla Melnetta are consistent with this assumption. These ages are so young with respect to the timing of LGM deglaciation that it is unlikely that $^{10}$Be from earlier exposures is present (Ivy-Ochs et al., 2006, 2007; Kelly et al., 2006).

422 Radiocarbon dates from peat bogs in and near the Engadine suggest that the inner Alpine ice-stream
423 network had already collapsed by about 16 – 17 cal ka (e.g. Suter, 1981; Burga, 1987; Studer,
424 2005). Taking the vertical proximity of the LGM ice surface into account, and assuming a simple
425 ice surface lowering scenario during deglaciation, one would expect older ages at this elevation and
426 position. We therefore hypothesise that a small ice-cap type glaciation remained at Bottas Glischas.
427 This ice configuration extended to the north slope towards Crap Alv Laiets. Here, Alb3, Alb4/1 and
428 Alb4/2 yielded $^{10}$Be ages of 11.2 ± 0.9, 11.9 ± 1.1 and 12.8 ± 0.8 ka (Table 6), with a mean age for
429 the deglaciation of this strongly eroded bedrock terrace of 12.0 ± 1.2 ka. We suggest that a local and
430 dynamically rather inactive glaciation remained after downwasting of the main LGM Engadine ice
431 dome. Due to its northerly exposure, a possible snow-drift input (lee-effect from Bottas Glischas)
432 and protection from solar radiation and wind erosion, perennial snow fields could have been of
433 great importance in helping maintain ice-cover. Similar $^{10}$Be dates were obtained at Nägelisgrätli in
434 the Grimsel region in central Switzerland (Ivy-Ochs, 1996; Kelly et al., 2006; Ivy-Ochs et al.,
435 2007).
436 The question arises, especially in the case of the uppermost level (Bottas Glischas, Fuorcla
437 Melnetta), whether there was a long-lasting ice mass until the beginning of the Bølling/Allerød-
438 interstadial or alternatively a complete melting of the ice followed by a reglaciation during the
439 Younger Dryas with a low erosional potential. This could have led merely to a temporary
440 interruption of production of $^{10}$Be without considerable subglacial erosion of the bedrock. Both
441 scenarios would result in similar exposure ages.
442 $^{10}$Be exposure ages for samples from the roche moutonnée Crap Alv are 12.6 ± 0.9 and 11.9 ± 1.6
443 ka (mean age: 12.3 ± 1.3 ka). This suggests ice recession from the site no later than 13.5 ka when
444 errors on the oldest age are included. Palynological investigations from a peat bog situated within
445 the roche moutonnée area Crap Alv (c. 100 m away from the exposure dating sampling sites; see
446 Fig. 1) suggest bog formation prior to the beginning of the Allerød period (Maisch, 1981), that is

447 before 13.9 ka (Hadorn et al., 2002; Hajdas et al., 2004). The moraines just down-valley of the Crap
448 Alv bedrock site have been assigned to the Daun stadial which has been interpreted as pre-Bolling
449 in age (Maisch, 1981) and thus older than 14.7 ka (see also section 2.2). The surface of the roche
450 moutonnée Crap Alv has well-preserved glacial polish so that subsequent spalling can be ruled out.
451 Due to the position of the roche moutonnée below the timberline, an influence from vegetation
452 cannot be ruled out. However, the effect of shielding by trees and leaves on the local $^{10}$Be
453 production rate is generally estimated to be less than 4% (Cerling and Craig, 1994; Plug et al.,
454 2007). To obtain ages that would assign the roche moutonnée Crap Alv to the Daun-stadial (> 14.7
455 ka), unrealistically high amounts of snow would be necessary. On the other hand we cannot rule out
456 that the bedrock was covered by 10 - 20 cm of till at least during part of its exposure that would
457 have decreased nuclide production by more than 10% (Ivy-Ochs, 1996). Little additional
458 information is gleaned from the basal radiocarbon date (Maisch, 1981) from the peat bog at Crap
459 Alv which is 10550 - 11400 cal yr BP (calibrated using Oxcal 4.1; Bronk Ramsey, 2001; Reimer et
460 al., 2009) and simply records the onset of the Holocene. At present, we do not have a plausible
461 explanation for the contradictory findings between the numerical dating and the palynological
462 results. Unfortunately, the data from boulder Cra1 does not help us solve this problem, as the $^{10}$Be
463 age is only 4.8 ± 0.5 ka. The Cra1 moraine is located approximately 3 km away from the LIA
464 moraine (Maisch, 1981) and has an associated ELA depression of 220 - 230 m, which classifies it as
465 Egesen stadial moraine. The obtained $^{10}$Be exposure age probably reflects toppling or exhumation
466 of the boulder. The LIA moraine, upstream of this site, represents the Holocene maximum glacier
467 extent in this catchment. Another possibility would be that the mapped 'Daun' moraines represent
468 an early stage of the Younger Dryas and that the sediment, which was assigned to a pre-Allerød
469 age, is a remnant of a bog that was later overridden by a glacier during the Younger Dryas. Several
470 findings support this hypothesis: all numerical dating results ($^{10}$Be and $^{14}$C) suggest ice decay at this

point during the Younger Dryas. Furthermore, the ELA calculations give only slightly higher values than those usually obtained for the Younger Dryas period.

*4.3.2. Val Mulix*

We could locate only one boulder suitable for exposure dating on the Daun moraine fragments at the former confluence point of Val Tschitta and the Val Mulix glacier. Boulder VM7 yielded an age of 14.9 ± 1.8 ka. This age is in good accord with the assignment of the moraine to the Daun stadial, based on the geomorphological mapping of Maisch (1981). Although the sample was taken from a very large boulder > 1.5 m above ground level and near the moraine crest, at least partial post-depositional exhumation and an intermittent influence of vegetation are possible. We therefore interpret the age as a minimum age. Overturning of the block can be ruled out due to its size. Compared to the other boulder samples, we included here a higher value for snow coverage due to its relatively sheltered position and the presence of vegetation reducing the influence of wind and allowing snow cover to last longer. This age is, furthermore, supported by the dating results of the soil that developed on this moraine (14.3 ± 2.3 ka; Egli et al., 2010).

The largest boulder on the upper right lateral moraine in the Val Mulix has a $^{10}$Be age of 14.7 ± 1.2 ka (VM1). Based on overall shape and ELA depression the moraine is classified as an Egesen I stadial moraine (Maisch, 1981), which implies that the obtained age is too old. A possible scenario, besides pre-exposure, would be that deposition occurred towards the end of the Oldest Dryas (Daun stadial) and this lateral moraine was not affected by the following Egesen stadial readvances during the Younger Dryas (there the moraines were accumulated laterally). In this case the age of VM1 would represent a minimum age of a Daun moraine that was then reoccupied during the Younger Dryas. This moraine, being a composite moraine formed as a result of multiple glacier advances could also explain the pronounced sharp-crested moraine morphology, which is not typical for isolated Daun moraines. They normally have a rather rounded shape and often show a solifluction

overprint. Reoccupation of lateral moraines and boulders of early deposited sediment protruding through later deposits have been recognised by Briner (2009) and Licciardi et al. (2004) based on $^{10}$Be data. Notably, our weathering rind measurements support the hypothesis that this moraine could contain boulders deposited before the Younger Dryas. The marked difference between the weathering rind values of the upper Egesen I (mean/median: 4.6 mm/4.0 mm) and the Egesen II moraine (mean/median: 3.1 mm/3.1 mm) is high and cannot be explained by the formation of two moraine sets within a few hundred years.

Two boulders were dated from a fragment of the Egesen II left lateral moraine. VM11 (10.7 ± 0.9 ka) gives an age that is in line with ages obtained in other studies (Ivy-Ochs et al., 1996, 2009a: Julierpass, Switzerland; Federici et al., 2008: Maritime Alps, Italy; Hormes et al., 2008: Northern Italy). The age of 15.4 ± 1.3 ka (VM6) on the same moraine is clearly too old. The moraine is located inside of the Egesen I stadial. Having an ELA depression of 125 m (Maisch, 1981), it falls in the Egesen II substadial. In contrast to the Egesen I right lateral moraine discussed above, which is a large ridge moraine and found high on the flanks of the valley (elevation ≥ 2150 m a.s.l.), the Egesen II moraine is nearly at the valley floor. This allows us to rule out that this moraine is a reoccupied Daun stadial moraine. Pre-exposure must be assumed in this case. This picture does not change even when corrections for snow and erosion are left out.

Boulders VM2 (8.7 ± 0.6 ka) and VM5 (12.8 ± 1.1 ka) were sampled on the uppermost and the lowermost part of the relict rock glacier, respectively (Fig. 2A). VM2 is a large flat-topped boulder and snow coverage was therefore assumed to be slightly higher than on VM5 (see Table 6). As VM2 is relatively close to the debris source, it could give a rough idea about the cessation of rock glacier activity. Nevertheless, considering the relatively dense lichen growth on the boulder, the highly developed vegetation coverage on the nearby debris cones and on the headwall itself, a deposition age much later than the inactivation of the rock glacier seems to be rather unlikely. Assuming that VM5 (12.8 ± 1.1 ka) was not subject to pre-exposure in the bedrock setting, it could

521 have been deposited initially on either the Lower Egesen I right lateral moraine or the Daun
522 moraine fragment that is located parallel to and just upslope of the lower Egesen I moraine (shown
523 as dashed line in Fig. 2A). A boulder situated on the still-existing part of the Daun moraine was
524 sampled but not measured successfully (VM3; see Figs. 1, 2). Boulder VM5 was then incorporated
525 in the rock glacier as it moved downhill. This would be in agreement with its position near the front
526 of the rock glacier. The volume of the boulder (c. 12 $m^3$) and its big base area makes a relatively
527 stable position plausible despite being on the surface of the rock glacier even during the active.
528 Recognising that part of the boulders exposure may have been at higher elevation than its present
529 location and that the orientation may not have been constant we take the age of boulder VM5 to
530 approximate the time that has elapsed since its deposition on the now destroyed (breached) moraine.
531 We note that spending the first few thousand years exposed at an elevation a few hundred meters
532 higher would decrease the age by only a few percent. If the age of the boulder therefore also
533 includes the travel time on the rock glacier we may estimate the mean annual deformation rate of
534 the rock glacier. Considering the travel distance of about 650 m, the age difference of 4000 years
535 between VM2 and VM5 yields a mean annual deformation rate of the rock glacier of approximately
536 16 cm. Horizontal displacements in the range of decimetres are common for active rock glaciers, as
537 shown by aerial photogrammetry and direct deformation measurements (e.g. Kääb et al., 1997;
538 Arenson et al., 2002). A pre-condition for this interpretation is that the boulder VM5 began to move
539 soon after its deposition on the moraine. The age of boulder VM4 (10.8 ± 0.9 ka) on the lower
540 Egesen I moraine, which was also cut by the rock glacier, shows that this cannot have been the case.
541 The ice must have disappeared before the rock glacier started to move. Consequently, based on a
542 shorter activity phase (about 2000 - 3000 years), a deformation rate that is about twice as high
543 (around 30 cm/year) must be assumed. This is still in the range of rock glacier surface velocities
544 reported as being typical in the literature (Haeberli et al., 2006). VM4 is slightly younger than one
545 would expect for this position. Yet, taking the error range into account, a correspondence with the

546 inner Egesen moraine (11.3 ± 0.6 ka) at the nearby Julierpass (Ivy-Ochs et al., 1996, 2006, 2009a)
547 and with the Great Aletsch Glacier (10.6 to 11.9 ka, recalculated by Ivy-Ochs et al., 2008, based on
548 data in Kelly et al., 2004) is possible. These moraines are similar in morphologic character and ELA
549 depression to the Egesen II moraine in Val Mulix.
550 Two bedrock samples were taken at Sur La Crappa to determine how long upper Val Mulix has
551 been ice-free. VM10 (taken from the glacially polished bedrock at Sur la Crappa) yields an
552 exposure age of 11.9 ± 0.9 ka. VM8, yielding 9.0 ± 0.7 ka, was sampled at a c. 40 m lower position,
553 closer to the theoretical central flow line of the past glacier (Fig. 1). As there is no evidence of
554 glacier advance in the younger time period at this site, we postulate differences in snow coverage or
555 possibly even shielding due to a thin cover of glacial sediments during the early part of exposure
556 may account for the difference in ages from a contemporaneous bedrock surface. From these
557 samples taken only a few hundreds of metres down-valley from the moraines of 1850 AD, we
558 conclude that the main ice body in the Val Mulix already downwasted very quickly to a near-1850
559 size by the end of the Lateglacial without large-scale re-advances afterwards. This supports the
560 general concept of a Holocene glacier fluctuation pattern, which oscillated in only a very small
561 spatial range (see also Maisch, 1987; Maisch et al., 2000).
562
563 **5. Conclusions**
564
565 In this study we tried to reconstruct and validate the temporal framework of the Lateglacial and
566 early Holocene landscape development in the Val Mulix and the Albula region in eastern
567 Switzerland. The main aim was to increase the database of absolute ages of glacial and periglacial
568 landforms in the Alps and to cross-check the results with different relative dating methods. The
569 geomorphologic map of Maisch (1981) served as a basis for the identification of the sampling sites
570 and provided guidance for the interpretation. Numerical and relative dating techniques verified the

571 general findings of Maisch (1981) but provided some new, process-related insights into the
572 landscape evolution.
573 Regarding the Lateglacial and early Holocene landscape evolution and glacial history, we obtained
574 the following main findings:
575 (1) In both regions, a detailed and appropriate resolution of geomorphic processes within the
576 Lateglacial was not possible using Schmidt-hammer rebound values. This method, however, proved
577 to be a helpful tool in distinguishing landforms over the longer Holocene timeframe. Considering
578 other studies conducted on nearby Holocene surfaces (active rock glaciers with the same lithology)
579 and combining them with the findings of this work, the following R-value ranges seem to be
580 typical: 30 - 40 for Lateglacial to early Holocene-aged surfaces, 40 - 50 for early Holocene to mid-
581 Holocene-aged surfaces and 50 - 60 for increasingly younger and even modern surfaces (root zone
582 of active rock glaciers and 1850 AD moraine). These value ranges are comparable with results of
583 Shakesby et al. (2006) and Engel (2007). Engel (2007) reported that R-values from granitic surfaces
584 lower than 29 can be assigned to pre-LGM landforms (Czech Republic). This would fit well with
585 the time-dependent correlation of the R-values in the Albula region.
586 (2) Taking the exposure dating results and the geomorphological map into consideration,
587 weathering rind measurements generally yielded meaningful results along the proposed timeline.
588 This method showed its potential to support the reconstruction of the chronology of Lateglacial and
589 early Holocene sequences.
590 (3) The strategy of a combined application of relative and numerical dating techniques should be
591 pursued. It provides the possibility of building up calibration curves for relative methods that have
592 at least local validity. The relative methods – in particular the weathering rind approach – in turn
593 may strengthen/weaken numerical ages and can provide some level of verification in cases of doubt,
594 especially when only a low number of dates is available. For instance, the weathering rind thickness
595 mean/median values in the case of the upper Egesen I moraine supports the hypothesis that the

596 moraine was initially deposited during the Daun stadial and then was reoccupied during the Egesen
597 stadial (Younger Dryas), as indicated by the exposure age of VM1.
598 (4) In the Albula region, exposure ages from the transfluence Bottas Glischas (maximum 13.5 ± 1.4
599 ka), from the Fuorcla Melnetta (13.5 ± 1.4 ka) and from Crap Alv Laiets (mean age: 12.0 ± 1.2 ka)
600 do not support a simple LGM ice surface lowering model as interpreted from pollen and
601 radiocarbon ages. This would require older exposure ages. We suggest the ages reflect the influence
602 of a long-lasting local glaciation or even a reglaciation during the Younger Dryas and/or thick
603 perennial snow cover.
604 (5) The suggested Daun age of the moraine formed by the confluence of the former Val Mulix and
605 the Val Tschitta glacier can be supported with a $^{10}$Be exposure age of 14.9 ± 1.8 ka (sample VM7).
606 An age of 14.7 ± 1.2 from a boulder on the Val Mulix upper Egesen moraine implies reoccupation
607 of a moraine that was originally formed during the Daun stadial. Both dates strengthen the
608 hypothesis that glacier advances of the Daun stadial occurred during the Oldest Dryas before the
609 onset of the Bølling warm interval.
610 (6) A $^{10}$Be age of 10.8 ± 0.9 ka for the only boulder on the Val Mulix lower Egesen moraine points
611 to formation and final moraine stabilisation at the end of the Younger Dryas similar to other Egesen
612 stadial moraines in the Alps.
613 (7) $^{10}$Be ages in combination with the morphostratigraphic situation suggest a main active phase of
614 the relict rock glacier between the end of the Younger Dryas and the early Holocene. The
615 estimation of the mean annual deformation rate is, however, difficult. Nonetheless, our calculations
616 yield c. 30 cm, which is typical for rock glaciers of such environments.
617 (8) The $^{10}$Be ages measured at the rock barrier near the LIA moraine (11.9 ± 0.9 ka and, at a lower
618 position, 9.0 ± 0.7 ka) directly record when Val Mulix was ice-free. Although the dataset is limited,
619 these ages can be seen as direct evidence for the generally assumed (but rarely proven) rapid ice-

retreat at the end of the Younger Dryas and for the subsequent Holocene glacier length variations, which have been reduced to a small spatial range.

## 6. Acknowledgements

This study was supported by the Swiss National Science Foundation grants numbers 20-109565/1 and 20-124380 and the 'Stiftung für wissenschaftliche Forschung an der Universität Zürich'. We are, furthermore, indebted to R. Waldmeier and S. Heer for their support during the field campaigns. We would like to thank S. Binnie and two anonymous reviewers for their helpful comments on an earlier version of this manuscript.

## References

Arenson, L., Hoelzle, M., Springman, S., 2002. Borehole Deformation and Internal Structure of Some Rock Galciers in Switzerland. Permafrost and Periglacial Processes 13, 117-135.

Auer, M., 2003. Regionalisierung von Schneeparametern – Eine Methode zur Darstellung von Schneeparametern im Relief. Publikation Gewässerkunde 304.

Balco, G., Stone, J.O., Lifton, N. A., Dunai, T. J., 2008. A complete and easily accessible means of calculating surface exposure ages or erosion rates from $^{10}$Be and $^{26}$Al measurements. Quaternary Geochronology 3, 174-195.

Bearth, P., Heierli, H, Roesli, F., 1987. Geologischer Atlas der Schweiz, Blatt 1237 Albulapass (Atlasblatt 81). Schweizerische Geologische Kommission und Landeshydrologie und –geologie (Eds.).

644 Bini, A., Buoncristiani, J.F., Couterrand, S., Ellwanger, D., Felber, M., Florineth, D., Graf, H.R.,
645 Keller, O., Kelly, M., Schlüchter, C., Schoeneich, P., 2009. Die Schweiz während des
646 letzteiszeitlichen Maximums (LGM). Map 1:500000. Bundesamt für Landestopographie
647 swisstopo (Ed.).
648 Briner, J.P., 2009. Moraine pebbles and boulders yield indistinguishable $^{10}$Be ages: A case study
649 from Colorado, USA. Quaternary Geochronology 4, 299–305.
650 Bronk Ramsey, C., 2001. Development of the radiocarbon calibration program OxCal. Radiocarbon
651 43, 355-363.
652 Brown, E.T., Edmond, J.M., Raisbeck, G.M., Yiou, F., Desgarceaux, S., 1992. Effective attenuation
653 length of cosmic rays producing $^{10}$Be and $^{26}$Al in quartz: implications for surface exposure
654 dating. Geophysical Research Letters 9, 369-372.
655 Burga, C.A., 1987. Gletscher und Vegetationsgeschichte der Sudrätischen Alpen seit der
656 Späteiszeit. Denkschriften der Schweizerischen Naturforschenden Gesellschaft 101.
657 Castelli, S., 2000. Geomorphologische Kartierung im Gebiet Julierpass, Val Suvretta und Corvatsch
658 (Oberengadin, GR), sowie Versuche zur Relativdatierung der morphologischen Formen mit der
659 Schmidt-Hammer Methode. Diploma thesis, University of Zurich, Switzerland.
660 Cerling, TE, Craig, H. 1994., Geomorphology and in-situ cosmogenic isotopes: Annual Review of
661 Earth an Planetary Sciences 22, 273-317.
662 Chinn, T.J.H., 1981. Use of rock weathering-rind thickness for Holocene absolute age-dating in
663 New Zealand. Arctic and Alpine Research 13, 33-45.
664 Chmeleff, J., von Blanckenburg, F., Kossert, K., and Jakob, D., 2010. Determination of the $^{10}$Be
665 half-life by multicollector ICP-MS and liquid scintillation counting, Nuclear Instruments and
666 Methods B 268, 192-199
667 Cockburn, H.A.P., Summerfield, MA., 2004. Gemorphological applications of cosmogenic isotope
668 analysis. Progress in Physical Geography 28, 1-42.

669 Colman, S.M., Pierce, K.L., 1981., Weahtering rinds on andesitic and basaltic stones as a
670 Quaternary age indicator, western United States. US Geological Survey Professional Paper 1210.
671 Compeer, M., 2009. Datierung von Blockgletschern und Bodenentwicklung auf spätglazialen
672 Oberflächen. Geomorphologische und bodenkundliche Untersuchungen im Gebiet des
673 Albulapasses. Diploma thesis, University of Zurich, Switzerland.
674 Cornelius, H.P., 1929. Geologische Karte der Err-Julier-Gruppe, Spezialkarte Nr. 115.
675 Cornelius, H.P., 1935. Geologie der Err-Julier-Gruppe. Beiträge zur Geolog. Karte der Schweiz,
676 N.F., 70. Lief., 1. Teil (Das Baumaterial).
677 Cossart, E., Fort, M., Bourles, D., Carcaillet, J., Perrier, R., Siame, L., Braucher, R., 2010. Climatic
678 significance of glacier retreat and rockglaciers re-assessed in the light of cosmogenic dating and
679 weathering rind thickness in Clarée valley (Briançonnais, French Alps). Catena 80, 204-219.
680 Day, M.J., Goudie, A.S., 1977. Field assessment of rock hardness using the Schmidt hammer.
681 British Geomorphological Research Group, Technical Bulletin 18, 19-29.
682 Dunne, J., Elmore, D., Muzikar, P., 1999. Scaling factors fot the rates of production of cosmogenic
683 shielding and attenuation at depth on sloped surfaces. Geomorphology 27, 3-11.
684 EDI (Eidgenössisches Departement des Innern), 1992. Hydrologischer Atlas der Schweiz.
685 Landeshydrologie und -geologie, Bern, Switzerland.
686 Egli, M., Brandová, D., Böhlert, R. Favilli, F., Kubik, P., 2010. $^{10}$Be inventories in Alpine soils and
687 their potential for dating land surfaces. Geomorphology 119, 62-73.
688 Engel, Z., 2007. Measurement and age assignement of intact rock strength in the Krkonose
689 Mountains, Czech Republic. Annals of Geomorphology 51(Suppl. 1), 69-80.
690 Federici, P.R., Granger, D.E., Pappalardo, M., Ribolini, A., Spagnolo, M., Cyr, A.J., 2008.
691 Exposure age dating and Equilibrium Line Altitude reconstruction of an Egesen moraine in the
692 Maritime Alps, Italy. Boreas 37, 245-253.

693 Florineth, D., 1998. Surface geometry of the Last Glacial Maximum (LGM) in the southeastern
694 Swiss Alps (Graubünden) ant its paleoclimatic significance. Eiszeitalter und Gegenwart 48, 23-
695 37.
696 Florineth, D., Schlüchter S., 2000. Alpine Evidence for Atmospheric Circulation Patterns in Europe
697 during the Last Glacial Maximum. Quaternary Research 54, 295-308.
698 Frauenfelder R., 2005. Regional-scale modelling of the occurrence and dynamics of rock glaciers
699 and the distribution of paleopermafrost. Schriftenreihe Physische Geographie 45. Haeberli W,
700 Maisch M (Eds.), Institute of Geography, University of Zurich.
701 Frauenfelder, R., Laustela, M., Kaeaeb A., 2005. Relative age dating of Alpine rock glacier
702 surfaces. Annals of Geomorphology 49(2), 145-166.
703 Gordon, S.J., Dorn, R.I., 2005., In situ weathering rind erosion. Geomorphology 67, 97-113.
704 Gosse, J.C., Klein, J., Evenson, E.B., Lawn, B., Middleton, R., 1995. Beryllium-10 dating of the
705 duration and retreat of the last Pinedale glacial sequence. Science 268, 1329-1333.
706 Gosse, J.C., Phillips, F.M., 2001. Terrestrial in situ produced cosmogenic nuclides: Theory and
707 application. Quaternary Science Reviews 20, 1475-1560.
708 Götze, J. Kleeberg, R., Wiedemann, P., Plötze, M., Angélica, R.S., 2004. Mineralogical
709 characterization of kaolin from the Capim region, Pará State (Brazil). Applied Mineralogy -
710 Developments in Science and Technology v2, p.685-688; Pecchio, M. et al. (eds.); ICAM-BR;
711 Sao Paulo.
712 Gross, G., Kerschner, H., Patzelt, G., 1977. Methodische Untersuchungen über die Schneegrenze in
713 alpinen Gletschergebieten. Zeitschrift für Gletscherkunde und Glazialgeologie 12, 223-251.
714 Hadorn P., Thew N., Coope G.R., Lemdahl G., Hajdas I., Bonani G., 2002. A Late-Glacial and
715 early Holocene environment and climate history for the Neuchâtel region (CH). In: Richard H,
716 Vignot A (eds.) Equilibres et Ruptures dans les écosystèmes depuis 20 000 ans en Europe de
717 l'Ouest. Collection Annales Littéraires Série Environment, Sociétés et Archéologie 3, 75-90.

718 Haeberli, W., Brandovà, D., Burga, C., Egli, M., Frauenfelder, R., Kääb, A., Maisch, M., 2003.
719 Methods for absolute and relative age dating of rock-glacier surfaces in alpine permafrost. In:
720 Proceedings of the Eighth International Conference on Permafrost, 21-25 July 2003, Zurich,
721 Switzerland. A.A. Balkema Publishers, Vol. 1, pp. 343-348
722 Haeberli, W., 2004. Glaciers and ice caps: historical background and strategies of world-wide
723 monitoring. In: Mass balance of the cryosphere, Bamber, J.L., Payne, A.J. (Eds.), Cambridge
724 University Press, Cambridge, pp. 559-578.
725 Haeberli, W., Hallet, B., Arenson, L., Elconin, R., Humlum, O., Kääb, A., Kaufmann, V., Ladanyi,
726 B., Matsouka, N., Springman, S., Vonder Mühll, D., 2006. Permafrost creep and rock glacier
727 dynamics. Permafrost and periglacial processes 17, 189-214.
728 Hajdas I., Bonani, G., Hadorn, P., Thew, N., Coope, G. R., Lemdahl, G., 2004. Radiocarbon and
729 absolute chronology of the Late-Glacial record from Hauterive/Rouges-Terres, Lake Neuchâtel
730 (CH). Nuclear Instruments and Methods in Physics Research Section B: Beam Interactions with
731 Materials and Atoms 223-224, 308-312.
732 Heuberger, H., 1966. Gletschergeschichtliche Untersuchungen in den Zentralalpen zwischen
733 Sellrain und Ötztal. Wissenschaftliche Alpenvereinshefte 20. Universitätsverlag Wagner,
734 Innsbruck.
735 Hormes, A., Ivy-Ochs, S., Kubik, P.W., Ferreli, L., Michetti, A.M., 2008. $^{10}$Be exposure ages of a
736 rock avalanche and a late glacial moraine in Alta Valtellina, Italian Alps. Quaternary
737 International 190, 136-145.
738 Ivy-Ochs, S., 1996., The dating of rock surfaces using in situ produced $^{10}$Be, $^{26}$Al and $^{36}$Cl, with
739 examples from Antarctica and the Swiss Alps. PhD Thesis, ETH Zurich, No. 11763.
740 Ivy-Ochs, S., Schlüchter, C., Kubik, P.W., Synal, H.A., Beer, J., Kerschner, H., 1996. The exposure
741 ages of an Egesen moraine at Julier Pass, Switzerland, measured with the cosmogenic
742 radionuclides $^{10}$Be, $^{26}$Al and $^{36}$Cl. Eclogae geologicae helvetiae 89(3), 1049-1063.

743 Ivy-Ochs, S., Schäfer, J., Kubik, P.W., Synal, H.A., Schlüchter, C., 2004., The timing of
744 deglaciation on the northern Alpine foreland (Switzerland). Eclogae Geologicae Helvetiae 97,
745 47-55.
746 Ivy-Ochs, S., Kerschner, H., Reuther, A., Maisch, M., Sailer, R., Schaefer, J., Kubik, P.W., Synal,
747 H.A., Schlüchter, C., 2006. The timing of glacier advances in the northern European Alps based
748 on surface exposure dating with cosmogenic $^{10}$Be, $^{26}$Al, $^{36}$C and $^{21}$Ne. In: In Situ-Produced
749 Cosmogenic Nuclides and Quantification of Gelogical Processes: Geological Society of America
750 Special Paper 415, Siame, L.L., Bourlès, D.L., Brown, T.T. (Eds.). Geological Society of
751 America, pp. 43-60.
752 Ivy-Ochs, S., Kerschner, H., Schlüchter, C., 2007. Cosmogenic nuclides and the dating of
753 Lateglacial and Early Holocene glacier variations: The Alpine perspective. Quaternary
754 international 164–165, 53-63. doi: 10.1016/j.geomorph.2007.10.024
755 Ivy-Ochs, S., Kerschner, H., Reuther, A., Preusser, F., Heine, K., Maisch, M., Kubik, PW.,
756 Schlüchter, C., 2008. Chronology of the last glacial cycle in the European Alps. Journal of
757 Quaternary Science 23(6-7), 559-573.
758 Ivy-Ochs, S., Kerschner., H., Maisch, M., Christl, M., Kubik, P.W., Schlüchter, C., 2009a. Latest
759 Pleistocene and Holocene glacier variations in the European Alps. Quaternary Science Reviews
760 28, 2137-2149. Doi:10.1016/j.quascirev.2009.03.009
761 Ivy-Ochs, S., Poschinger, A.V., Synal, H.A., Maisch, M., 2009b. Surface exposure dating of the
762 Flims landslide, Graubünden, Switzerland. Geomorphology 103, 104-112.
763 Ivy-Ochs, S., Schaller, M., 2010. Examining processes and rates of landscape change with
764 cosmogenic radionuclides. In: Froehlich, K. (Editor), Environmental Radionuclides: Tracers and
765 Timers of Terrestrial Processes. Elsevier (in press).
766 Jenkins, R., 1999. X-ray Fluorescence Spectrometry. Wiley-VCH, 2nd edition.

767 Kääb, A., Haeberli, W., Gudmundsson, G.H., 1997. Analysing the Creep of Mountain Permafrost
768 using High Precision Aerial Photogrammetry: 25 Years of Monitoring Gruben Rock Glacier,
769 Swiss Alps. Permafrost and Periglacial Processes 8, 409-426.
770 Keller, O., Krayss E., 1993. The Rhine-Linth Glacier in the upper Würm: A model of the last
771 Alpine glaciation. Quaternary International 18, 15-27.
772 Keller, O., Krayss, E., 2005. Der Rhein-Linth-Gletscher im letzten Hochglazial. Vierteljahresschrift
773 der Naturforschenden Gesellschaft in Zürich 150(1-2), 19-32.
774 Kellerer-Pirklbauer, A., 2008. The Schmidt-Hammer as a Relative Age Dating Tool for Rock
775 Glacier Surfaces: Examples from Northern and Central Europe. Proceedings of the Ninth
776 International Conference on Permafrost, University of Alaska Fairbanks, pp. 913-918.
777 Kellerer-Pirklbauer, A., Wangensteen, B., Farbrot, H., Etzelmüller, B., 2008. Relative surface age-
778 dating of rock glacier systems near Hólar in Hjaltadalur, northern Iceland. Journal of Quaternary
779 Science 23(2), 137-151.
780 Kelly, M.A., Kubik, P.W., von Blanckenburg, F., Schlüchter, C., 2004. Surface exposure dating of
781 the Great Aletsch Glacier Egesen moraine system, western Swiss Alps, using the cosmogenic
782 nuclide $^{10}$Be. Journal of Quaternary Science 19, 431-441.
783 Kelly, M.A., Ivy-Ochs, S., Kubik, P.W., von Blanckenburg, F., Schlüchter, C., 2006. Chronology of
784 deglaciation based on 10Be dates of glacial erosional features in the Grimsel Pass region, central
785 Swiss Alps. Boreas 35, 634-643.
786 Kerschner, H., 1978. Untersuchungen zum Daun- und Egesenstadium in Nordtirol und Graubünden
787 (methodische Überlegungen). Geographischer Jahresbericht aus Österreich 36, 26-49.
788 Kerschner, H., Berktold, E., 1982. Spätglaziale Gletscherstände und Schuttformen im Senderstal,
789 nördliche Stubaieralpen, Tirol. Zeitschrift für Gletscherkunde und Glaziologie 17, 125-134.
790 Kerschner, H., Ivy-Ochs, S., Schlüchter, C., 1999. Paleoclimatic interpretation of the early late-
791 glacial glacier in the Gschnitz valley, central Alps, Austria. Annals of Glaciology 28, 135-140.

792 Kohl, C.P., Nishiizumi, K., 1992. Chemical isolation of quartz for measurement of in-situ produced
793 cosmogenic nuclides. Geochimica et Cosmochimica Acta 56, 3583-3587.
794 Kubik, P.W., Christl, M., 2010. $^{10}$Be and $^{26}$Al measurements at the Zurich 6 MV Tandem AMS
795 facility. Nuclear Instruments and Methods B 268, 880-883
796 Korschinek, G., Bergmaier, A., Faestermann, T., Gerstmann, U.C., Knie, K., Rugel, G., Wallner,
797 A., Dillmann, I., Dollinger, G., Lierse von Gostomski, Ch., Kossert, K., Maiti, M., Poutivtsev,
798 M., and Remmert, A., 2010. A new value for the half-life of $^{10}$Be by Heavy-Ion Elastic Recoil
799 Detection and liquid scintillation counting, Nuclear Instruments and Methods. B 268, 187-191
800 Lal, D., 1988. In situ-produced cosmogenic isotopes in terrestrial rocks. Annual Review of Earth
801 and Planetary Sciences 16, 355-388.
802 Lal, D., 1991. Cosmic ray labeling of erosion surfaces: in-situ nuclide production rates and erosion
803 models. Earth and Planetary Science Letters 104, 424–439.
804 Laustela, M., 2003. Messung und Analyse von Verwitterungsrinden zur relativen Altersdatierung
805 ausgewählter Blockgletscher in den Bündner Alpen. Diploma thesis, University of Zurich,
806 Switzerland.
807 Laustela, M., Egli, M., Frauenfelder, R., Kaeaeb, A., Maisch, M., Haeberli, W., 2003. Weathering
808 rinds measurements and relative age dating of rockglacier surfaces in crystalline regions of the
809 Eastern Swiss Alps. In: Permafrost, Phillips, Springman and Arenson (Eds.), Swets & Zeitlinger,
810 Lisse, pp. 627-632.
811 Licciardi, J.M., Clark, P.U., Brook, E.J., Elmore, D., Sharma, P., 2004. Variable responses of
812 western U.S. glaciers during the last deglaciation. Geology 32, 81–84.
813 Maisch, M. 1981., Glazialmorphologische und gletschergeschichtliche Untersuchungen im Gebiet
814 zwischen Landwasser- und Albulatal (Kt. Graubünden, Schweiz). Physische Geographie 3. Dept.
815 of Geography, University of Zurich.

816 Maisch, M., 1987. Zur Gletschergeschichte des alpinen Spätglazials: Analyse und Interpretation
817 von Schneegrenzdaten. Geographica Helvetica, 42, 63-71.
818 Maisch, M., Wipf, A., Denneler, B., Battaglia, J, Benz, C., 2000. Die Gletscher der Schweizer
819 Alpen. Gletscherhochstand 1850, aktuelle Vergletscherung, Gletscherschwund-Szenarien.
820 Schlussbericht NFP 31 Projekt, vdf-Hochschulverlag ETH Zürich.
821 Masarik, J., Frank, M., Schaefer, J.M., Wieler, R., 2001. Correction of in-situ cosmogenic nuclide
822 production rates for geomagnetic field intensity variations during the past 800,000 years.
823 Geochimica et Cosmochimica Acta 65, 2995-3003.
824 Masarik, L,, Wieler, R., 2003., Production rates of cosmogenic nuclides in boulders. Earth an
825 Planetary Science Letters 216, 201-208.
826 Matsouka, N., Ikeda, A., 2001. Geological control on the distribution and characteristics of talus-
827 derived rock glaciers. Annual Report of the Institute of Geosciences, University of Tsukuba,
828 Japan 27, 11-16.
829 Matthews, J.A., Shakesby, R.A., 1984. The status of the "Little Ice Age" in Southern Norway;
830 relative age dating of Neoglacial moraines with Schmidt hammer and lichenometry. Boreas
831 13(3), 333-346.
832 McCarroll, D., 1987. The Schmidt hammer in geomorphology: five sources of instrument error.
833 British Geomorphology Research Group Technical Bulletin 36, 16-27.
834 Nesje, A., Blikra, L.H., Anda, E., 1994. Dating rockfall-avalanche deposits from degree of rock-
835 surface weathering by Schmidt-hammer tests: a study from Norangsdalen, SunnmØre, Norway.
836 Norwegian Journal of Geology 74(2), 108-113.
837 Nishiizumi, K., Imamura, M., Caffee, M.W., Southon, J.R., Finkel, R.C., and McAninch, J., 2007.
838 Absolute calibration of $^{10}$Be AMS standards, Nuclear Instruments and Methods. B 258, 403-413

839 Oerlemans, J., Anderson, B., Hubbard, A., Huybrechts, P., Johannesson, T., Knap, W.H., Schmeits,
840 M., Stroeven, A.P., van de Val, R.S.W., Wallinga, J., Zuo, Z., 1998. Modelling the response of
841 glaciers to climate warming. Climate dynamics 14, 267-274.
842 Oguchi, C.T., 2001. Formation of weathering rinds on andesite. Earth Surface Processes and
843 Landforms 26, 847-858.
844 Penck, A., Brückner, E., 1901/1909. Die Alpen im Eiszeitalter. 3 volumes, Leipzig, Tauchnitz.
845 Pfiffner, O.A., 2009. *Geologie der Alpen*. Haupt Verlag, Bern/Stuttgart/Wien, 359 pp.
846 Pigati, J.S., Lifton, N.A., 2004. Geomagnetic effects on time-integrated cosmogenic nuclide
847 production with emphasis on in situ $^{14}C$ and $^{10}Be$. Earth and Planetary Science Letters 226 (1-2),
848 193-205.
849 Plötze, M., Trausch Giudici, I. Messerklinger, S., Springman, S., 2003. Swiss Lacustrine Clay:
850 Mineralogical and mechanical characteristics. In: Vermeer, Schweiger, Karstunen, Cudny (eds.),
851 Int. Workshop on Geotechnics of Soft Soils-Theory and Practice, Noordwijkerhout, VGE, pp.
852 473-478.
853 Plug, L., Gosse, J., West, J., Bigley, R., 2007. Attenuation of cosmic ray flux in temperate forest.
854 Journal of Geophysical Research 112, F02022, doi:10.1029/2006JF000668.
855 Putkonen, J., Swanson, T., 2003. Accuracy of cosmogenic ages for moraines. Quaternary Research
856 59, 255-261.
857 Reimer, P.J., Baillie, M.G.L., Bard, E., Bayliss, A., Beck, J.W., Blackwell, P.G., Bronk Ramsey, C.,
858 Buck, C.E., Burr, G.S., Edwards, R.L., Friedrich, M., Grootes, P.M., Guilderson, T.P., Hajdas, I.,
859 Heaton, T.J., Hogg, A.G., Hughen, K.A., Kaiser, K.F., Kromer, B., McCormac, F.G., Manning,
860 S.W., Reimer, R.W., Richards, D.A., Southon, J.R., Talamo, S., Turney, C.S.M., van der Plicht,
861 J., Weyhenmeyer, C.E., 2009. INTCAL09 and MARINE09 radiocarbon age calibration curves,
862 0-50,000 years cal BP. Radiocarbon 51, 1111-1150.

Reuther, A.U., Ivy-Ochs, S., Heine, K., 2006. Application of surface exposure dating in glacial geomorphology and the interpretation of moraine ages. Annals of Geomorphology 142, 335-359.

Schaefer, J.M., Denton, G.H., Kaplan, M., Putnam, A., Finkel, R.C., Barrell, D.J.A., Andersen, B.G, Schwartz, R., Mackintosh, A., Chinn, T., Schlüchter, C., 2009. High-frequency Holocene glacier fluctuations in New Zealand differ from the northern signature. Science 324, 622-625.

Schlüchter, C., 2004., The Swiss glacial record – A schematic summary. In: Quaternary Glaciations- Extent and chronology, Part I: Europe. Ehlers, J., Gibbard, P.L. (Eds.), Elsevier, London, pp. 413-418.

Schmidt, E., 1951. A Non-destructive concrete tester. Concrete 59(8), 34-35.

Schwarb, M., Daly, C., Frei., C, Schär., C., 2000. Mittlere jährliche Niederschlagshöhe im europäischen Alpenraum 1971-1990. In Hydrologischer Atlas der Schweiz, Blatt 2.6.

Shakesby, R.A., Matthews, J.A., Owen, G., 2006. The Schmidt hammer as a relative-age dating tool and its potential for calibrated-age dating in Holocene glaciated environments. Quaternary Science Reviews 25, 2846-2867.

Stone, J.O., 2000. Air pressure and cosmogenic isotope production. Journal of Geophysical Research 105/B10(23), 753-759.

Stone, J.O. and Ballantyne C., K., 2006. Dimensions and deglacial chronology of the Outer Hebrides Ice Cap, northwest Scotland: implications of cosmic ray exosure dating. Journal of Quaternary Science 21 (1), 75-84

Studer, M. 2005. Gletschergeschichtliche Untersuchungen und geomorphologische Kartierung im Raum Maloja-Val Forno. Ein Beitrag zur regionalen Landschaftsgeschichte. Diploma thesis, University of Zurich, Switzerland.

Suter, J., 1981. Gletschergeschichte des Oberengadins: Untersuchung on Gletscherschwankungen in der Err-Julier-Gruppe. Physische Geographie 2, Institute of Geography, University of Zurich, Switzerland.

888 Whitehouse, I.E., McSaveney, M.J., Knuepfer, P.L.K., Chinn, T.J.H., 1986. Growth of weathering
889 rinds on Torlesse sandstone, southern Alps, New Zealand. In: Rates of Chemical Weathering of
890 Rocks and Minerals, Colman, S.M., Dethier, D.P. (Eds.), Academic Press: Orlando, pp. 419-435.
891 Winkler, S., 2000. The little ice age maximum in the Southern Alps, New Zealand: preliminary
892 results at Mueller Glacier. The Holocene 10, 643-647.
893 Winkler, S., 2005. The 'Schmidt hammer' as a relative-age dating technique: potential and
894 limitations of its application on Holocene moraines in Mt Cook National Park, Southern Alps,
895 New Zealand. New Zealand Journal of Geology and Geophysics 48, 105-116.
896 Winkler, S., Shakesby, R.A., 1995. Anwendung von Lichenometrie und Schmidt-Hammer zur
897 relativen Altersdatierung prä-frührezenter Moränen am Beispiel der Vorfelder von Guslar-,
898 Mitterkar-, Rofenkar- und Vernagtferner (Ötztaler Alpen/Österreich). Petermanns
899 Geographische Mitteilungen 139, 283-304.

## Figure captions

Fig.1. Map of the Val Mulix and the region near the Albulapass showing the glacial geomorphology based on Maisch (1981). Names of sampling sites are given in white frames. Sampling codes of $^{10}$Be-samples (VM, Alb, Cra) match Table 1 and are included in order to ease readability.

Fig. 2. A: View from Sur la Crappa down to the Val Mulix. Moraines and the relict rock glacier are indicated with white lines. Samples from moraines are marked with rectangles, samples from the rock glacier with triangles. B: Sampled boulder on the lower Egesen I moraine. C: The transfluence saddle at Bottas Glischas seen from the helicopter. D: Overview of the bedrock sampling sites in the Albula region. The picture was taken from the roche moutonnée Crap Alv.

Fig. 3. $^{10}$Be ages calculated for Alb2 with different amounts of snow and erosion rates (1, 2 and 3 mm/ka). The slope of the graphs shows the high influence of snow coverage on the measured age. An increase from 0.2 to 1.0 m snow for 6 months per year leads to roughly 1000 years older ages. The erosion rate has a comparatively small effect on the age.

Fig. 4. Schematic presentation of Schmidt-hammer R-values from different landforms measured in the Albula region and in the adjacent Julier area (same lithology) with an approximate temporal assignment. Data is compiled from different authors: a = this study; b = Compeer (2009); c = Frauenfelder et al. (2005); d = Laustela (2003); e = Castelli (2000)

Fig. 5. Histograms of the measured weathering rind thicknesses. Mean and median values are given in each case.

Fig. 6. Relief (source: DHM25, Swisstopo) with the sampling locations and corresponding $^{10}$Be ages (ka). Rounded ages with the lower snow correction values are given (see Table 6, scenario C).

**Figure 1**

**Click here to download high resolution image**

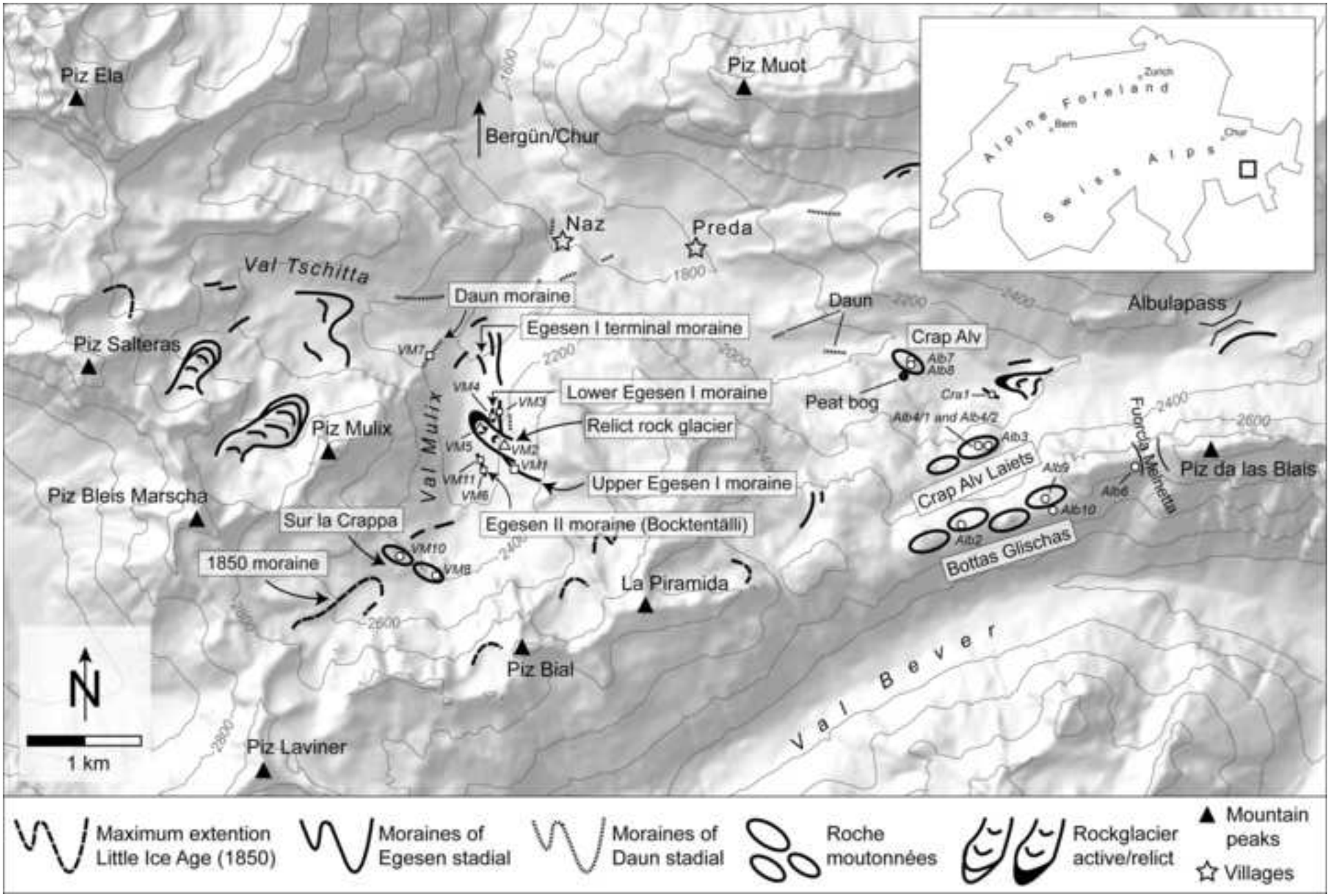

**Figure 2**

Click here to download high resolution image

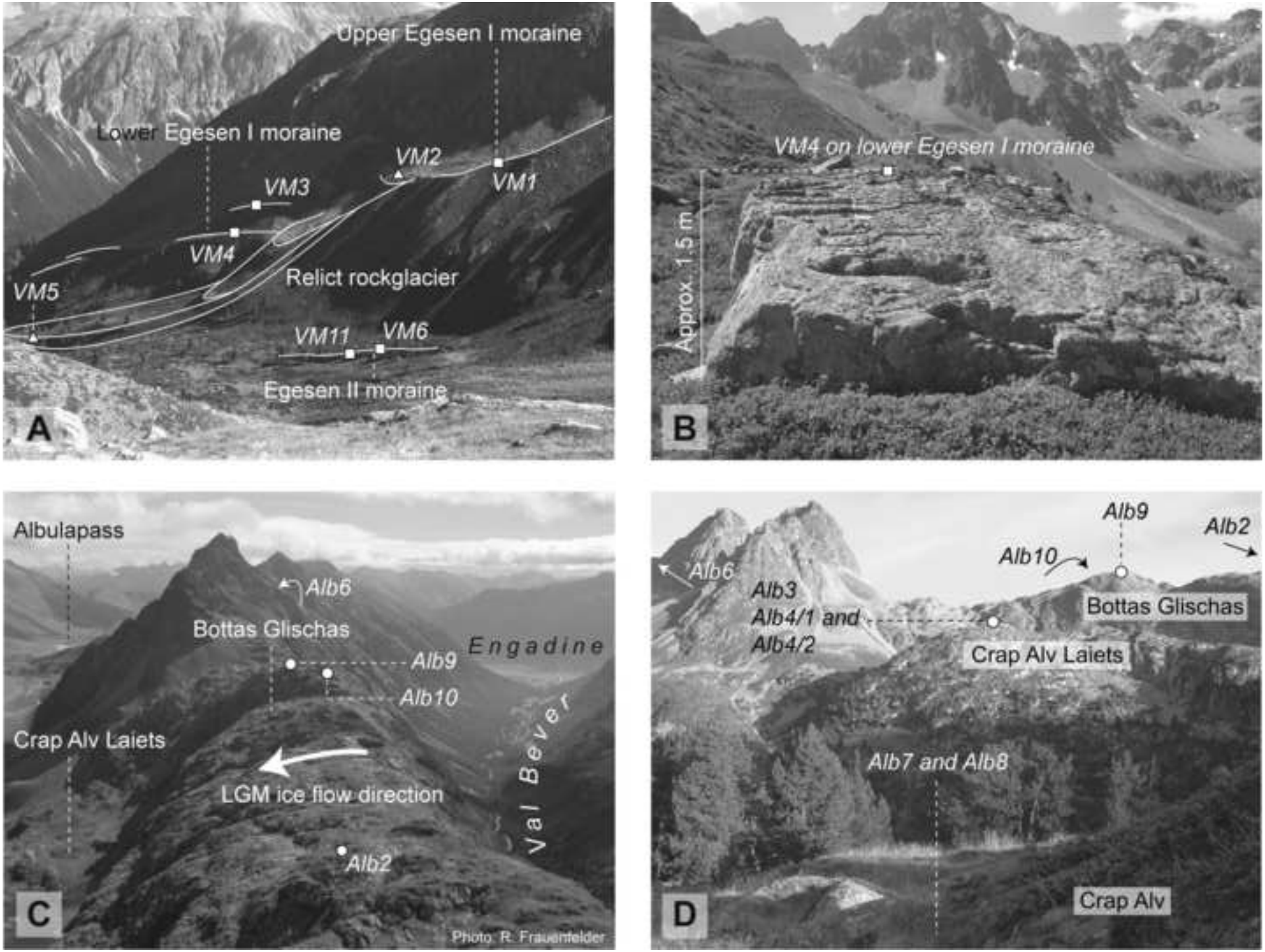

Figure 3
Click here to download high resolution image

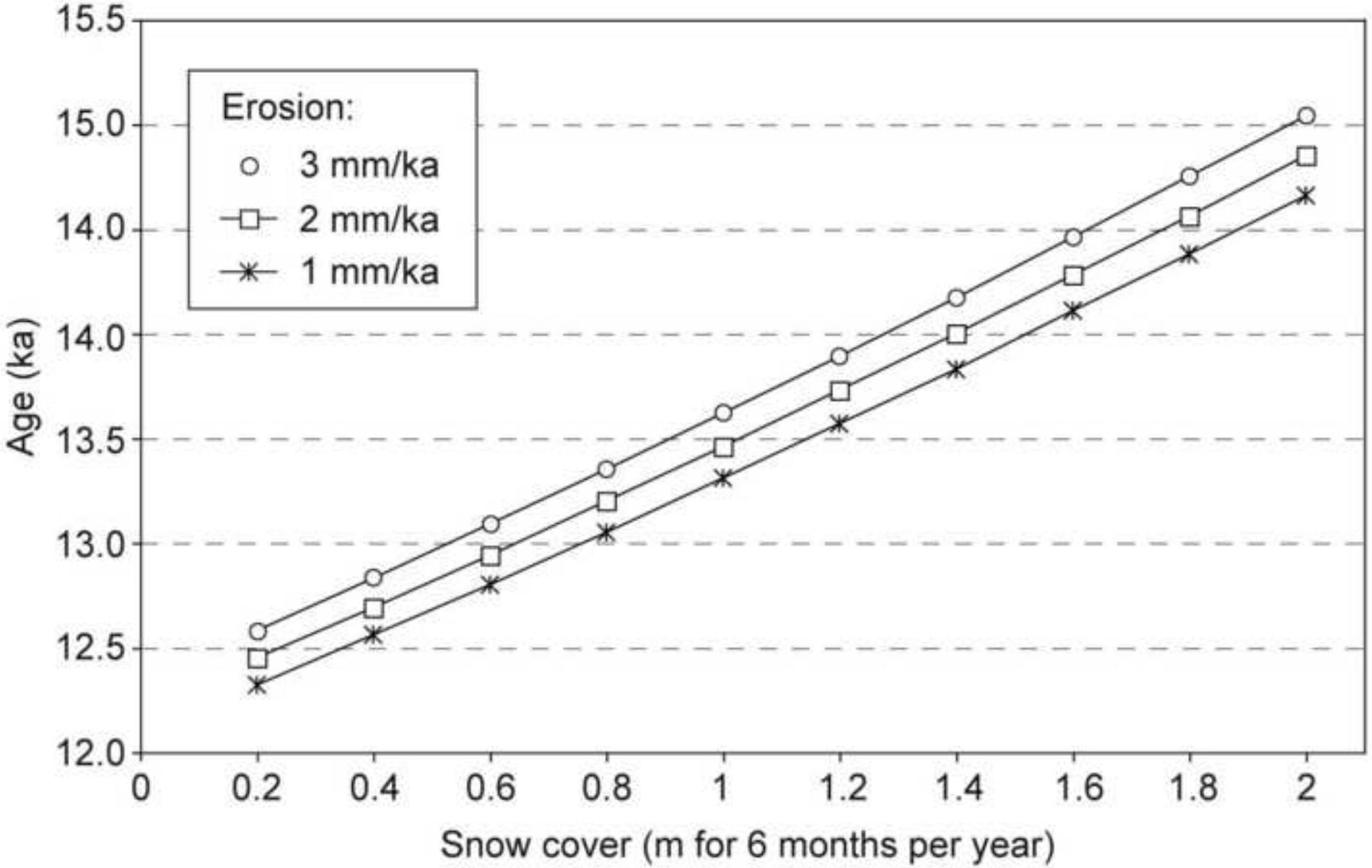

Figure 4

Click here to download high resolution image

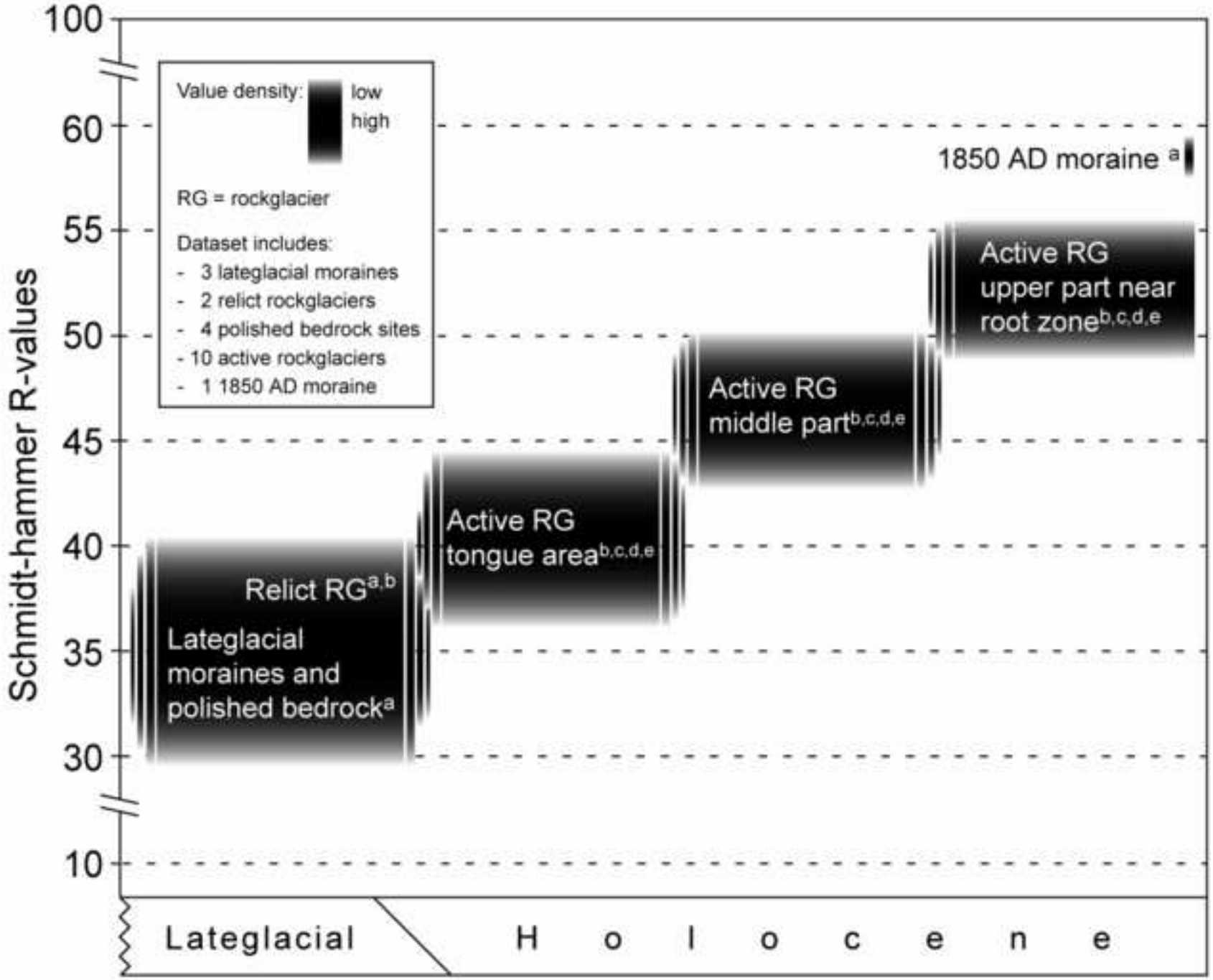

**Figure 5**

**Click here to download high resolution image**

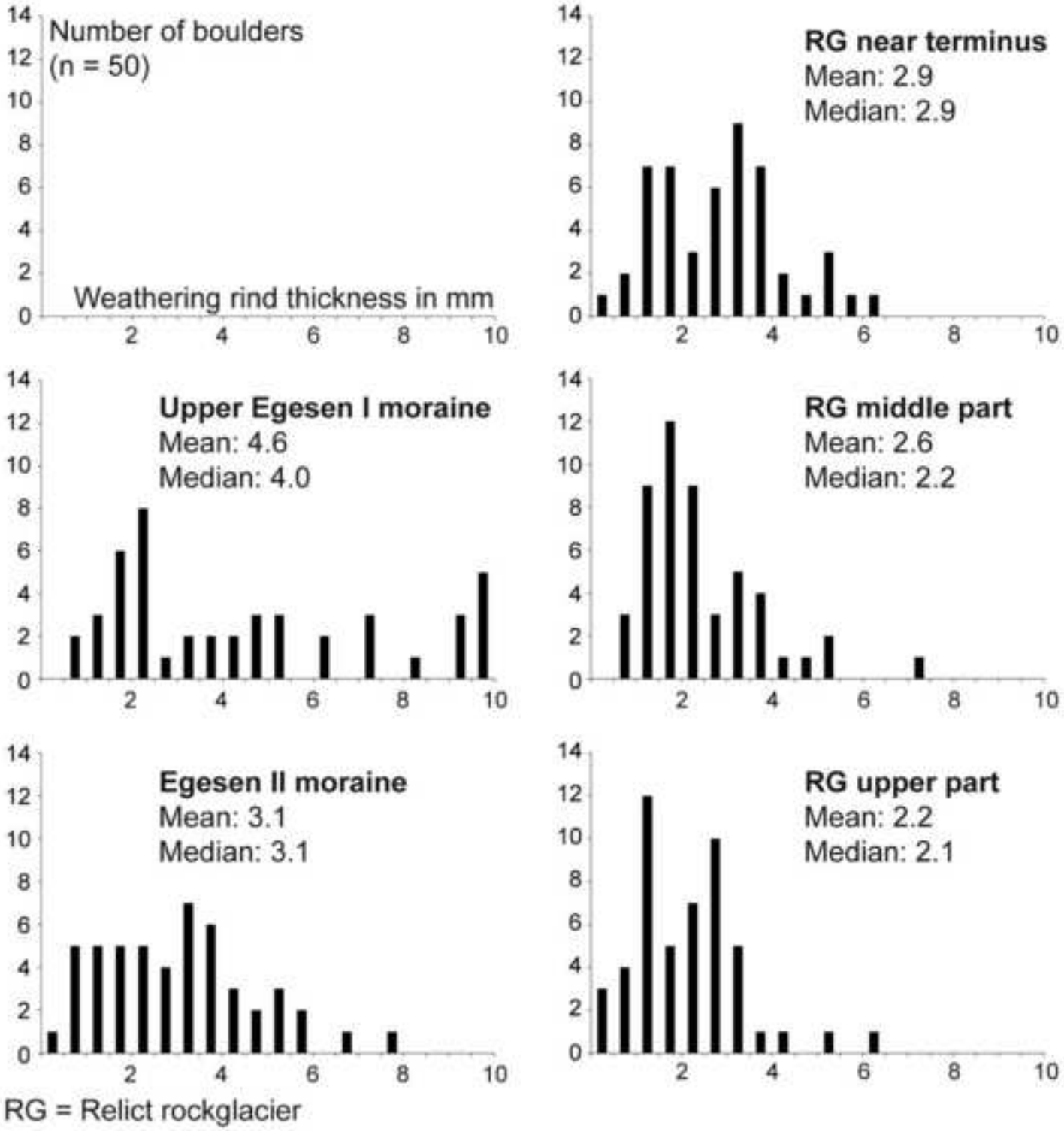

Figure 6
Click here to download high resolution image

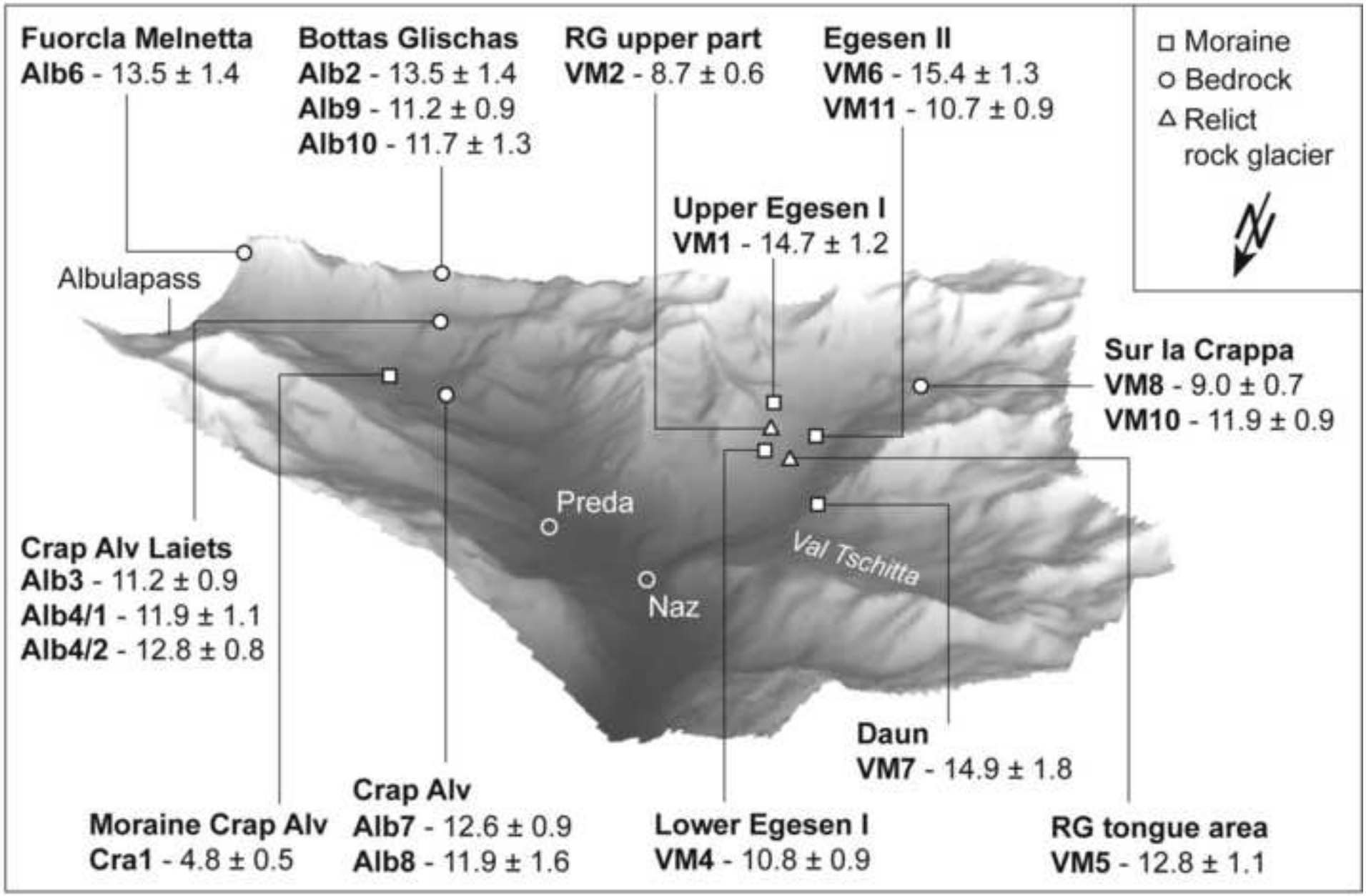

**Table 1**

Table 1
Overview of localities and applied methods. In case of moraines, locality names are according to Maisch (1981) and should be understood as tentative assignments.

| Method | Sample Code | AMS Code | Localities | Altitude (m asl) |
|---|---|---|---|---|
| SED using $^{10}$Be | VM 1 | Mulix I ZB5787 | Upper Egesen I moraine | 2320 |
| SED using $^{10}$Be | VM 2 | Mulix II ZB5578 | Relict rock glacier, lobe in the uppermost part | 2280 |
| SED using $^{10}$Be | VM 4 | Mulix IV ZB5579 | Lower Egesen I moraine | 2150 |
| SED using $^{10}$Be | VM 5 | Mulix V ZB5580 | Relict rock glacier, lobe near terminus | 2080 |
| SED using $^{10}$Be | VM 6 | Mulix VI ZB5581 | Egesen II moraine (Bocktentälli) | 2145 |
| SED using $^{10}$Be | VM 7 | Mulix VII ZB5788 | Daun moraine | 2120 |
| SED using $^{10}$Be | VM 8 | Mulix VIII ZB7156 | Sur la Crappa, polished bedrock | 2423 |
| SED using $^{10}$Be | VM 10 | Mulix X ZB6321 | Sur la Crappa, polished bedrock | 2460 |
| SED using $^{10}$Be | VM 11 | Mulix XI ZB7157 | Egesen II moraine (Bocktentälli) | 2145 |
| SED using $^{10}$Be | Alb 2 | Alb II ZB5944 | Bottas Glischas, polished bedrock | 2570 |
| SED using $^{10}$Be | Alb 3 | Alb III ZB5945 | Crap Alv Laiets, polished bedrock | 2325 |
| SED using $^{10}$Be | Alb 4/1 | Alb IV/I ZB5946 | Crap Alv Laiets, polished bedrock | 2320 |
| SED using $^{10}$Be | Alb 4/2 | Alb IV/II ZB5948 | Crap Alv Laiets, polished bedrock | 2320 |
| SED using $^{10}$Be | Alb 6 | Alb VI ZB7158 | Fuorcla Melnetta, polished bedrock | 2680 |
| SED using $^{10}$Be | Alb 7 | Alb VII ZB5949 | Crap Alv, polished bedrock | 2060 |
| SED using $^{10}$Be | Alb 8 | Alb VIII ZB5950 | Crap Alv, polished bedrock | 2070 |
| SED using $^{10}$Be | Alb 9 | Alb IX ZB7159 | Bottas Glischas, polished bedrock | 2607 |
| SED using $^{10}$Be | Alb 10 | Alb VIII ZB7160 | Bottas Glischas, polished bedrock | 2585 |
| SED using $^{10}$Be | Cra1 | Alb VIII ZB7223 | Crap Alv moraine | 2055 |
| Schmidt-hammer | — | — | All polished bedrock sites; Relict rock glacier at all elevation levels; Upper Egesen I moraine; Egesen I terminal moraine; Egesen II moraine (Bocktentälli); 1850 AD moraine | — |
| Weathering rinds | — | — | Relict rock glacier at all elevation sites; Upper Egesen I moraine; Egesen II moraine (Bocktentälli) | — |

Table 2

Measured Schmidt-hammer rebound values. Standard error is given according to Winkler (2000). Where not specially indicated, 50 measurements per landform were performed. All measurements were performed on the same type of granite.

| Localities Val Mulix | 1850 AD moraine | Sur la Crappa | Egesen II moraine | Upper Egesen I moraine | Terminal Egesen I moraine | RG upper part | RG middle part | RG lower part |
|---|---|---|---|---|---|---|---|---|
| Mean value | 58.0 ± 1.9 | 37.8 ± 1.8 | 36.8 ± 2.1 | 35.6 ± 2.0 | 41.0 ± 2.1 | 37.5 ± 2.2 | 37.9 ± 2.2 | 37.9 ± 2.1 |

| Localities Albula | Crap Alv (n = 150) | Crap Alv Laiets (n = 150) | Bottas Glischas (n = 100) |
|---|---|---|---|
| Mean value | 39.5 ± 1.9 | 34.3 ± 1.9 | 33.3 ± 1.8 |

RG = rock glacier

**Table 3**

Table 3. Chemical composition of the investigated granites (“Albula granite”).

| Site | CaO g/kg | MgO g/kg | $K_2O$ g/kg | $Na_2O$ g/kg | $Al_2O_3$ g/kg | $Fe_2O_3$ g/kg | $SiO_2$ g/kg | MnO g/kg | $P_2O_5$ g/kg | $TiO_2$ g/kg | $ZrO_2$ g/kg | LOI g/kg |
|---|---|---|---|---|---|---|---|---|---|---|---|---|
| VM7 | 25.0 | 12.6 | 23.1 | 31.0 | 149.3 | 38.4 | 670.8 | 0.79 | 1.24 | 5.01 | 0.21 | 25.1 |
| VM5 | 13.9 | 7.5 | 33.8 | 29.7 | 145.8 | 24.2 | 708.4 | 0.54 | 0.89 | 3.56 | 0.18 | 14.7 |
| VM4 | 12.8 | 11.8 | 31.8 | 31.3 | 152.5 | 30.2 | 696.6 | 0.58 | 0.95 | 4.38 | 0.24 | 18.6 |
| * | 47.2 | 6.9 | 22.6 | 30.2 | 154.6 | 33.6 | 663.9 | 0.52 | 0.92 | 3.76 | 0.18 | 15.9 |
| VM2 | 15.8 | 9.4 | 32.6 | 26.6 | 141.8 | 27.8 | 691.6 | 0.58 | 0.88 | 3.75 | 0.17 | 17.4 |
| Mean | 22.9 | 9.6 | 28.8 | 29.8 | 148.8 | 30.9 | 686.3 | 0.60 | 0.98 | 4.09 | 0.20 | 18.3 |
| SD | 14.4 | 2.5 | 5.5 | 1.9 | 5.1 | 5.4 | 18.5 | 0.11 | 0.15 | 0.60 | 0.03 | 4.1 |

LOI = loss of ignition ; * lobe in the middle part of the relict rock glacier

**Table 4**

Table 4. Mean mineralogical composition of the parent material (C horizons of soils developed on the middle and lower part of the rock glacier, the Daun moraine and the BC horizon of the soil on the Egesen moraine) with respect to the sand fraction.

| | Sand mean (%) | SD |
|---|---|---|
| Calcite | 0.3 | 0.3 |
| Chlorite | 7.2 | 1.0 |
| Epidote | 4.4 | 2.8 |
| Microcline | 13.2 | 2.2 |
| Mica | 11.8 | 0.9 |
| Plagioclase | 36.4 | 0.8 |
| Quartz | 26.8 | 1.6 |

SD = standard deviation

**Table 5**

Table 5
The measurements and calculated data presented in the form needed for the calculation of the exposure age using CRONUS. Sample density was taken as 2.65 g $cm^{-1}$, the erosion rate as 0.0003 cm yr-1 and $^{10}Be$ standard was 07KNSTD.

| Sample name | Latitude (°N) | Longitude (°E) | Elevation (m) | Sample thickness (cm) | Shielding correction | $^{10}Be$ concentrations (atoms $g^{-1}$) | Uncertainty in $^{10}Be$ conc. (atoms $g^{-1}$) |
|---|---|---|---|---|---|---|---|
| Alb2 | 46.568 | 9.806 | 2570 | 3 | 0.995 | 3.981E+05 | 4.048E+04 |
| Alb3 | 46.573 | 9.808 | 2325 | 5 | 0.980 | 2.743E+05 | 2.285E+04 |
| Alb4/1 | 46.574 | 9.807 | 2320 | 4.5 | 0.968 | 2.871E+05 | 2.595E+04 |
| Alb4/2 | 46.574 | 9.807 | 2320 | 3.5 | 0.985 | 3.155E+05 | 2.045E+04 |
| Alb6 | 46.573 | 9.826 | 2680 | 5 | 0.876 | 3.696E+05 | 2.511E+04 |
| Alb7 | 46.581 | 9.802 | 2060 | 4.5 | 0.977 | 2.567E+05 | 3.195E+04 |
| Alb8 | 46.581 | 9.802 | 2070 | 3.5 | 0.975 | 2.460E+05 | 3.706E+04 |
| Alb9 | 46.568 | 9.812 | 2607 | 5 | 0.999 | 3.350E+05 | 2.794E+04 |
| Alb10 | 46.568 | 9.813 | 2585 | 4.5 | 0.977 | 3.379E+05 | 3.757E+04 |
| Cra 1 | 46.579 | 9.811 | 2055 | 3 | 0.960 | 9.802E+04 | 1.004E+04 |
| VM1 | 46.574 | 9.758 | 2320 | 4.5 | 0.947 | 3.668E+05 | 2.935E+04 |
| VM2 | 46.574 | 9.758 | 2310 | 4.5 | 0.957 | 2.165E+05 | 1.612E+04 |
| VM4 | 46.578 | 9.756 | 2160 | 5 | 0.943 | 2.413E+05 | 1.957E+04 |
| VM5 | 46.578 | 9.753 | 2080 | 5 | 0.941 | 2.671E+05 | 2.208E+04 |
| VM6 | 46.573 | 9.754 | 2145 | 3.5 | 0.899 | 3.272E+05 | 2.778E+04 |
| VM7 | 46.583 | 9.748 | 2120 | 4 | 0.953 | 3.099E+05 | 3.789E+04 |
| VM8 | 46.566 | 9.748 | 2423 | 4.5 | 0.953 | 2.302E+05 | 1.889E+04 |
| VM10 | 46.566 | 9.744 | 2460 | 5 | 0.972 | 3.145E+05 | 2.237E+04 |
| VM11 | 46.574 | 9.753 | 2175 | 5 | 0.943 | 2.423E+05 | 2.076E+04 |

**Table 6**

Table 6
Cosmogenic nuclide concentrations and the calculated exposure ages for the Albula and Val Mulix samples. Ages were calculated using an erosion rate of 3 mm per 1000 years. To emphasize the influence of erosion and snow coverage, the uncorrected ages (A) are shown as well as ages with two different estimated snow heights (m for 6 months) (B, D) and, also combined with erosion (C, E).
Estimated errors are given on the 1σ level including measurement error and the uncertainties of altitude/latitude scaling, topography and thickness correction.

| | (A) | | (B) | (C) | | (D) | (E) |
|---|---|---|---|---|---|---|---|
| Sample name | $^{10}$Be date (years) (uncorrected) | Snow cover (m / 6 month) | $^{10}$Be date (years) (Corr. for snow) | $^{10}$Be date (years) (Erosion, snow) | Snow cover (m / 6 month) | $^{10}$Be date (years) (Corr. for snow) | $^{10}$Be date (years) (Erosion, snow) |
| Alb 2 | 12120 ± 1230 | 0.8 | 13090 ± 1330 | 13540 ± 1380 | 1.2 | 13600 ± 1380 | 14090 ± 1430 |
| Alb 3 | 10120 ± 840 | 0.8 | 10930 ± 910 | 11240 ± 940 | 1.2 | 11350 ± 940 | 11690 ± 970 |
| Alb 4/1 | 10720 ± 970 | 0.8 | 11570 ± 1050 | 11920 ± 1080 | 1.2 | 12020 ± 1090 | 12400 ± 1120 |
| Alb 4/2 | 11490 ± 740 | 0.8 | 12400 ± 800 | 12810 ± 830 | 1.2 | 12890 ± 840 | 13330 ± 860 |
| Alb 6 | 12070 ± 1210 | 0.8 | 13030 ± 1310 | 13480 ± 1350 | 1.2 | 13540 ± 1360 | 14020 ± 1410 |
| Alb 7 | 11340 ± 770 | 0.8 | 12240 ± 830 | 12640 ± 860 | 1.0 | 12480 ± 850 | 12890 ± 880 |
| Alb 8 | 10720 ± 1390 | 0.8 | 11580 ± 1500 | 11930 ± 1550 | 1.0 | 11800 ± 1530 | 12170 ± 1580 |
| Alb 9 | 10080 ± 840 | 0.8 | 10880 ± 910 | 11190 ± 930 | 1.0 | 11090 ± 920 | 11420 ± 950 |
| Alb 10 | 10510 ± 1170 | 0.8 | 11340 ± 1260 | 11680 ± 1300 | 1.0 | 11560 ± 1280 | 11910 ± 1320 |
| Cra 1 | 4360 ± 450 | 0.8 | 4700 ± 480 | 4760 ± 490 | 1.0 | 4790 ± 490 | 4850 ± 500 |
| VM 1 | 14010 ± 1120 | 0.1 | 14150 ± 1130 | 14680 ± 1170 | 0.3 | 14420 ± 1150 | 14980 ± 1200 |
| VM 2 | 8230 ± 610 | 0.3 | 8470 ± 630 | 8660 ± 640 | 0.5 | 8640 ± 640 | 8830 ± 660 |
| VM 4 | 10350 ± 840 | 0.2 | 10550 ± 860 | 10840 ± 880 | 0.4 | 10750 ± 870 | 11060 ± 900 |
| VM 5 | 12130 ± 1000 | 0.2 | 12360 ± 1020 | 12770 ± 1060 | 0.4 | 12600 ± 1040 | 13020 ± 1080 |
| VM 6 | 14700 ± 1250 | 0.1 | 14840 ± 1260 | 15430 ± 1310 | 0.3 | 15130 ± 1280 | 15740 ± 1340 |
| VM 7 | 13410 ± 1640 | 0.7 | 14340 ± 1750 | 14890 ± 1820 | 1.0 | 14760 ± 1800 | 15340 ± 1870 |
| VM 8 | 8150 ± 700 | 0.8 | 8800 ± 720 | 9000 ± 740 | 1.2 | 9150 ± 750 | 9360 ± 770 |
| VM 10 | 10700 ± 760 | 0.8 | 11560 ± 820 | 11910 ± 850 | 1.2 | 10590 ± 910 | 10800 ± 930 |
| VM 11 | 10290 ± 880 | 0.1 | 10380 ± 890 | 10670 ± 910 | 0.3 | 10590 ± 910 | 10800 ± 930 |